water

MDPI

*Article*

# Assessing Hydroclimatic Extremes in the Iberian Peninsula Under Future Emission Scenarios

**Cristina Andrade [1,2,*], André Fonseca [2], António Fernandes [2], Christoph Menz [3] and João A. Santos [2]**

[1] Natural Hazards Research Center (NHRC.ipt), Instituto Politécnico de Tomar, Quinta do Contador, Estrada da Serra, 2300-313 Tomar, Portugal
[2] Centre for the Research and Technology of Agroenvironmental and Biological Sciences, CITAB, Inov4Agro, Universidade de Trás-os-Montes e Alto Douro, UTAD, Quinta de Prados, 5000-801 Vila Real, Portugal; andre.fonseca@utad.pt (A.F.); acpf91@utad.pt (A.F.); jsantos@utad.pt (J.A.S.)
[3] Potsdam Institute for Climate Impact Research (PIK) e. V., Telegrafenberg A 31, 14473 Potsdam, Germany; christoph.menz@pik-potsdam.de
* Correspondence: c.andrade@ipt.pt; Tel.: +351-249-328-100

## Abstract

Hydroclimatic extremes are projected to intensify across the Iberian Peninsula (IP) under future climate change, challenging water resources, agriculture, and ecosystems. This study evaluates future conditions using mean precipitation plus three precipitation-based indices: Consecutive Dry Days (CDD), number of dry spells (CDDn), and R95pTOT (Very Wet Days). Projections used a high-resolution CHELSA-ISIMIP3b CMIP6 ensemble under three Shared Socioeconomic Pathways (SSP1–2.6, SSP3–7.0, and SSP5–8.5) and three future periods (2041–2060, 2061–2080, and 2081–2100). A hydroclimatic stress framework based on historical CDD and the fraction of the R95pTOT quintiles was applied at grid-cell and watershed scales. Precipitation declines substantially under SSP5–8.5 across southern and interior basins, exceeding 30% by 2100. Simultaneously, CDD is projected to increase, surpassing 90 consecutive dry days per year in parts of southern Iberia, whereas CDDn is projected to increase mainly across eastern and northeastern Iberia, while remaining stable or decreasing locally in southern regions. Projections of the fraction of R95pTOT indicate increasing precipitation concentration, especially across Mediterranean and southeastern regions. Combined hydroclimatic stress expands markedly under stronger forcing: by 2081–2100 under SSP5–8.5, the "Very High" class covers approximately 97% of the Guadalquivir, 95% of the Guadiana, and 65% of the Tagus basins. In contrast, the Douro shows a more moderate intensification, while the Ebro remains outside the "Very High" combined-stress class, although approximately 19% of its area reaches "High" stress. These findings identify river basins where the spatial coexistence of increasingly prolonged dry conditions and greater precipitation concentration may pose growing hydroclimatic challenges, providing a basis for basin-scale water-resource planning and climate adaptation.

**Keywords:** hydroclimatic extremes; consecutive dry days; number of dry spells; very wet days; hydroclimatic stress framework; river basin management; Coupled Model Intercomparison Project Phase 6 (CMIP6); Shared Socioeconomic Pathways (SSP1–2.6, SSP3–7.0, SSP5–8.5); Iberian Peninsula

Check for updates

Academic Editor: Maria Mimikou

Received: 30 July 2026
Revised: 9 September 2026
Accepted: 21 September 2026
Published: 24 September 2026

**Copyright:** © 2026 by the authors. Licensee MDPI, Basel, Switzerland. This article is an open access article distributed under the terms and conditions of the Creative Commons Attribution (CC BY) license.

## 1. Introduction

The Iberian Peninsula (IP) is a climate-change hotspot where drought, water scarcity, and precipitation extremes are projected to intensify under future warming [1–7]. These

changes have major implications for water availability, agriculture [8,9], ecosystems, and regional resilience, particularly in the semi-arid regions of southern and eastern Iberia [10,11]. The Peninsula is characterised by pronounced climatic and hydrological gradients, ranging from humid Atlantic to semi-arid Mediterranean regimes, which, together with its complex topography, generate strong spatial variability in hydroclimatic responses [12]. This heterogeneity is particularly relevant across major river basins, where uneven water availability and competing agricultural, urban, and ecological demands increase vulnerability to future climate change. Recent Köppen–Geiger projections further indicate a northward expansion of arid and semi-arid climates by the end of the century under high-emission scenarios [13]. Spatially detailed assessments at the river-basin scale are therefore needed to identify emerging vulnerabilities and support climate adaptation and water management [14].

Hydroclimatic risks are often assessed through individual drought or extreme-precipitation indicators [6,7,11,15]. At the same time, a growing body of literature has examined compound climate events in which interacting, simultaneous, or sequential extremes amplify impacts beyond those associated with individual hazards [16–19]. However, comparatively less attention has been given to the long-term spatial coexistence of prolonged dry conditions and increasingly concentrated precipitation regimes within the same geographical regions [20]. This distinction is particularly relevant in Mediterranean river basins because these two conditions do not need to occur simultaneously to create competing management requirements: increasing water-storage and supply needs during prolonged dry periods must coexist with sufficient storage, conveyance, and flood-management capacity for concentrated precipitation [8,10,12,14]. Assessing these pressures within a common spatial framework may therefore provide information that cannot be obtained by considering dry and wet extremes independently.

In this study, precipitation-defined hydroclimatic conditions are characterised using three complementary indices based on the Expert Team on Climate Change Detection and Indices framework (ETCCDI) [21]: Consecutive Dry Days (CDD), representing the maximum annual duration of uninterrupted dry conditions; the number of dry spells (CDDn), describing their recurrence and fragmentation; and the fraction of R95pTOT, representing the proportion of annual precipitation occurring on historically very wet days. These indices were selected because they provide physically interpretable information on dry-period persistence, recurrence, and precipitation concentration. Other indicators, such as the Standardised Precipitation Index (SPI) and Standardised Precipitation Evapotranspiration Index (SPEI), are widely used for drought assessment [20,22], but the present analysis focuses on precipitation-based metrics that allow these specific hydroclimatic characteristics to be examined directly.

Building on the individual projections of these indices, we develop a hydroclimatic stress framework that integrates CDD and the fraction of R95pTOT within a common spatial assessment. The framework identifies locations where prolonged dry conditions and precipitation concentration become jointly elevated under future climate conditions and distinguishes High and Very High combined hydroclimatic stress. Its added value lies in moving beyond separate assessments of dry and wet extremes to identify the spatial progression of combined stress within the same grid cells and river basins. Rather than representing compound events in the strict temporal sense, the framework characterises the long-term spatial coexistence of two complementary hydroclimatic pressures. This basin-scale perspective is particularly relevant for water-resource planning because prolonged dry conditions and concentrated precipitation can create competing requirements for water storage, supply security, reservoir operation, and flood management [2,8,10,12,14].

Accordingly, this study assesses projected changes in mean precipitation and hydroclimatic extremes across the IP using high-resolution CHELSA–ISIMIP3b CMIP6 projections

under SSP1–2.6, SSP3–7.0, and SSP5–8.5 [23] for three future periods: 2041–2060, 2061–2080, and 2081–2100. The analysis has three objectives: (i) to quantify the spatial and temporal evolution of CDD, CDDn, and the fraction of R95pTOT under increasing climate forcing; (ii) to identify the spatial coexistence and progression of elevated dry-condition persistence and precipitation concentration through the proposed hydroclimatic stress framework; and (iii) to evaluate these changes at the river-basin scale to identify watersheds where combined hydroclimatic stress may pose increasing challenges for future water management and adaptation.

## 2. Materials and Methods

### *2.1. Study Area*

The IP, located in southwestern Europe (Figure 1), encompasses diverse climatic zones, ranging from humid Atlantic to semi-arid Mediterranean regions. Its complex topography, including mountain ranges such as the Pyrenees and the Sierra Nevada, and its transitional location between mid-latitude and subtropical circulation systems make it especially sensitive to climate variability and change [24].

Hydrologically, the IP is organised around major transboundary river basins, including the Douro, Tagus, Ebro, Guadiana, and Guadalquivir (Figure 1, Table A1). These watersheds are socioeconomically vital, supporting irrigation, hydropower, urban consumption, and ecosystems. However, they are also highly vulnerable to both meteorological droughts and flash flooding, making them key units of analysis for future hydroclimatic risks associated with non-concurrent extremes. The basin-scale focus of this study aligns with the governance structures of the EU Water Framework Directive (WFD) and offers practical value for regional water planning [25].

To implement spatial climate risk assessment, the analysis is structured around hydrological units defined by the HydroBASINS dataset (available at https://www.hydrosheds.org/pages/hydrobasins, accessed on 30 June 2025, ref. [26]), with Level 5 delineation. This watershed-based approach enables assessment of projected hydroclimatic stress within hydrologically meaningful management units, facilitating interpretation of regional climate impacts in the context of water-resource planning and basin-scale adaptation strategies. Major Iberian watersheds included in the analysis are the Ebro, Tagus (Tajo/Tejo), Douro (Duero), Guadiana, Guadalquivir, Minho (Miño), Júcar, Segura, Tinto-Odiel, and the Internal Basins of Catalonia (Figure 1). These basins represent the primary hydrological entities supporting agriculture, energy, and municipal water supply systems across the IP.

### *2.2. Climate Model Data and Ensemble Construction*

To assess projected changes in precipitation and related hydroclimatic indices over the IP, daily precipitation data from nine Global Climate Models (GCMs) participating in the Coupled Model Intercomparison Project Phase 6 (CMIP6) were used [27]. The selected models comprise CanESM5, CNRM-CM6-1, CNRM-ESM2-1, EC-Earth3, IPSL-CM6A-LR, MIROC6, MPI-ESM1-2-LR, MRI-ESM2-0, and UKESM1-0-LL.

The original CMIP6 simulations were first processed within the Inter-Sectoral Impact Model Intercomparison Project Phase 3b (ISIMIP3b) [28–33]. ISIMIP3b applies a consistent bias-adjustment methodology to the GCM outputs and provides harmonised daily climate projections at a spatial resolution of 0.5°, thereby reducing systematic model biases while preserving the projected climate-change signal.

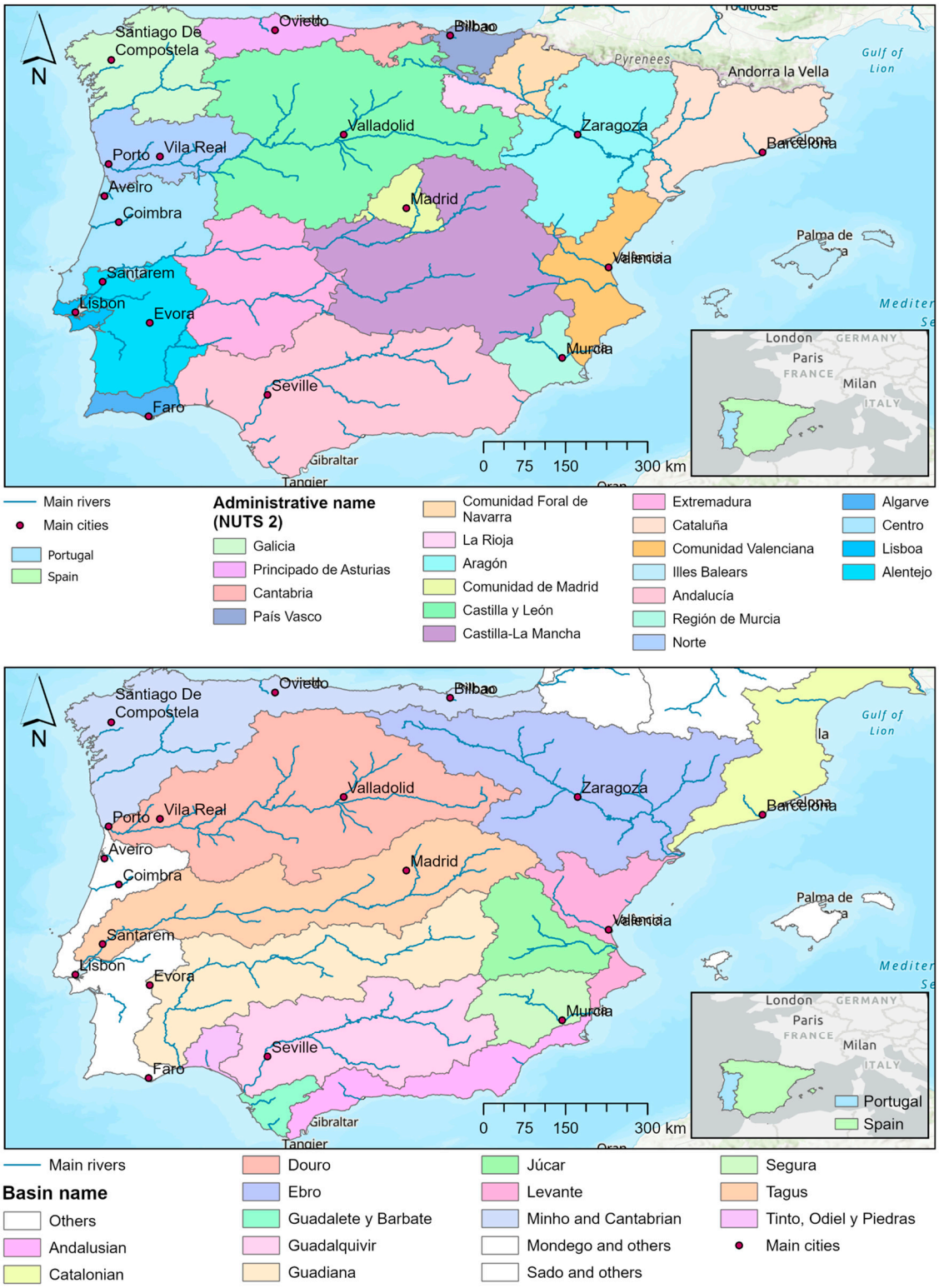



**Figure 1.** Maps of the Iberian Peninsula. **Top panel:** NUTS-2 administrative regions of Spain and Portugal, with major cities (red dots) and principal rivers (blue lines). The inset shows the location in southwestern Europe. **Bottom panel:** Major hydrographic basins (labelled) overlaid on the same geographic domain, with basin boundaries colour-coded and main cities for reference. Both panels include a 0–300 km scale bar and a north arrow.

The bias-adjusted ISIMIP3b climate projections were subsequently downscaled to a spatial resolution of 30 arc-seconds (approximately 1 km) using version 2.1 of the Climatologies at High Resolution for the Earth's Land Surface Areas (CHELSA) framework.

The CHELSA methodology [34,35] implements a quasi-mechanistic statistical–dynamical downscaling approach that explicitly accounts for fine-scale atmospheric–topographic interactions. Unlike purely statistical methods, CHELSA incorporates physically based processes, including orographic uplift and terrain-induced blocking, to improve the representation of near-surface climate over complex landscapes. This approach enables the generation of high-resolution climate fields while retaining the large-scale climatological consistency of the bias-adjusted ISIMIP3b projections and better representing local climatic variability in mountainous and heterogeneous terrain. The resulting dataset is hereafter referred to as the CHELSA–ISIMIP3b CMIP6 ensemble.

Model outputs were analysed for the historical baseline period (1991–2010) and three future time slices (2041–2060, 2061–2080, and 2081–2100) under three Shared Socioeconomic Pathways (SSP1–2.6, SSP3–7.0, and SSP5–8.5). The nine GCMs were selected based on the consistent availability of the required downscaled precipitation data within the CHELSA–ISIMIP3b dataset across the historical period and the three SSP scenarios considered.

### 2.3. Climate Indices and Pre-Processing

Based on the downscaled precipitation fields, the following climate indices were computed following the guidelines of the Expert Team on Climate Change Detection and Indices [33,36]:

- Consecutive Dry Days (CDD);
- Number of Dry Spells (CDDn);
- Very Wet Days (R95pTOT).

For each variable and index, the nine-model ensemble mean was calculated for the historical period and for each SSP–time-slice combination before the spatial analyses and classifications were performed. Furthermore, these indices were selected based on their interpretability, relevance for agriculture and water management, and widespread adoption in climate impact studies [1,37,38]. They were calculated on an annual basis and subsequently averaged over each 20-year time slice before assessing long-term changes. The analysis focuses primarily on ensemble-mean changes and does not evaluate grid-cell-level statistical significance; however, inter-model spread is explicitly assessed through the ensemble standard deviation, as described below.

To characterise inter-model uncertainty in the projected hydroclimatic indices, the standard deviation across the nine-member model ensemble was additionally calculated at each grid cell for CDD, CDDn, and the fraction of R95pTOT, for each SSP and future time slice (Figures A1–A3). These maps provide a spatial measure of the spread among individual model projections around the ensemble mean. The magnitude and spatial distribution of the standard deviation vary among indices, scenarios, and time horizons, with generally larger inter-model spread emerging under stronger radiative forcing and toward the end of the century, particularly for CDD. Accordingly, the ensemble-mean projections presented in the main analysis should be interpreted as central estimates of the multi-model response, while areas of larger standard deviation indicate lower model agreement on the magnitude of the projected changes. This uncertainty assessment does not constitute a formal probabilistic analysis or grid-cell-level significance test but provides an explicit indication of the robustness and spatial variability of the model ensemble underlying the projected hydroclimatic patterns.

Dry spell statistics provide insight into both duration and fragmentation of dry periods, relevant for crop resilience and soil moisture retention. In parallel, R95pTOT serves as a proxy for intense precipitation events and runoff generation potential, informing both flood risk and reservoir management. In this study, we analysed the fraction of R95pTOT, which is interpreted primarily as an indicator of precipitation concentration and, more

broadly, of rainfall-budget irregularity or volatility. Because it is expressed relative to annual precipitation, it does not directly quantify changes in the absolute intensity or amount of extreme rainfall. As a sensitivity test, the percentile thresholds used for classification were also calculated using the 30-year period 1981–2010 and compared with those derived from the 20-year historical baseline 1991–2010. The resulting 20th, 40th, 60th, and 80th percentile thresholds showed no material differences between the two reference periods, confirming that the classification is robust to the choice of the 20- versus 30-year baseline.

### *2.4. Hydroclimatic Stress Framework*

To assess future changes in hydroclimatic stress conditions across the IP, a classification framework based on the historical distributions of CDD and the fraction of R95pTOT was developed. Unlike compound-event approaches that explicitly analyse the temporal concurrence or sequential occurrence of extremes, the present framework evaluates projected changes in the maximum annual duration of uninterrupted dry conditions and the proportional concentration of annual precipitation on historically very wet days and combines them into a spatially integrated hydroclimatic stress indicator.

To characterise hydroclimatic extremes across the Peninsula, we employed a suite of precipitation-based indices that capture both dry conditions and precipitation concentration. These indices were selected based on their relevance to regional water stress dynamics, interpretability, and widespread use in climate impact studies. A brief description of each index and its role in the analysis is provided in Table 1.

**Table 1.** Definitions of the Hydroclimatic Indices used in this study (Note: $P_{y,d}$ denotes daily precipitation on day $d$ of year $y$; $L$ denotes the length of a sequence of consecutive dry days; $L_{y,j}$ is the duration of dry spell $j$; $N_y$ is the number of distinct dry spells in year $y$; $P_{95}$ denotes the 95th-percentile threshold of daily precipitation derived from the 1991–2010 historical baseline; and $\mathbf{1}(\cdot)$ is the indicator function, equal to 1 when the specified condition is satisfied and 0 otherwise).

| Index | Full Name | Units | Definition/Formula | Relevance |
|---|---|---|---|---|
| CDD | Consecutive Dry Days | days | Maximum number of consecutive days per year with daily precipitation < 1 mm $CDD_y = \max\left\{\mathrm{L} : P_{y,d} < 1 \text{ mm for L consecutive days}\right\}$ | Indicator of the maximum annual duration of uninterrupted dry conditions |
| CDDn | Number of Dry Spells | Periods/year | Annual count of dry spells exceeding five consecutive days (>5 days) with daily precipitation < 1 mm $CDDn_y = \sum_{j=1} \mathbf{1}\left(L_{y,j} > 5\right)$ | Captures dry-spell fragmentation and recurrence |
| Fraction of the R95pTOT | Fraction of the Very Wet Days | % of annual total | Percentage of annual precipitation occurring on days exceeding the grid-cell-specific 95th percentile of daily precipitation calculated over the 1981–2010 reference period $R95pTOT_y = 100\frac{\sum_d P_{y,d}\mathbf{1}\left(P_{y,d} > P_{95}\right)}{\sum_d P_{y,d}}$ | Measures the proportional contribution of historically very wet days to the annual precipitation budget |

For the calculation of R95pTOT, the 95th-percentile precipitation threshold ($P_{95}$) was determined independently at each grid cell from daily precipitation during the 30-year reference period 1981–2010. This grid-cell-specific threshold was subsequently held fixed when calculating R95pTOT for the historical and future periods. The 1981–2010 period used to derive $P_{95}$ should therefore be distinguished from the 1991–2010 historical climatological period used elsewhere in the analysis for comparison with the future 20-year time slices. The longer 30-year period was used specifically to provide a more representative reference distribution for estimating the percentile threshold.

The hydroclimatic stress framework is a threshold-based identification methodology. It was implemented through a simple classification approach based on the occurrence of the "Very High" categorical class derived independently from CDD and the fraction of R95pTOT. First, each index was classified into five quintile-based ordinal categories (20% intervals) ranging from 1 ("Very Low": 0 to 0.2) to 5 ("Very High": 0.8 to 1), according to the historical baseline distributions (1991–2010). Future projections were classified using the quintile thresholds derived from the historical baseline period (1991–2010), thereby enabling consistent comparison of hydroclimatic stress intensification across scenarios and time horizons. For each index, quintile thresholds were derived from the spatial distribution of the 1991–2010 climatological mean values across all Iberian grid cells, rather than independently from the temporal distribution at each grid cell. Combined hydroclimatic stress was then identified from the joint classification of CDD and the fraction of R95pTOT, focusing on grid cells in which both indices reached at least the "High" category (Class 4). Two levels of combined stress were distinguished. High hydroclimatic stress was assigned where both indices were classified as High or Very High but did not simultaneously reach the Very High category; this class therefore comprises the High–High (4–4), High–Very High (4–5), and Very High–High (5–4) combinations. "Very High" hydroclimatic stress was assigned exclusively where both CDD and the fraction of R95pTOT were classified as "Very High" (5–5). All remaining combinations were considered outside the "High" and "Very High" combined-stress classes (other).

This two-level classification extends the identification of hydroclimatic stress beyond the most restrictive joint upper-quintile condition while retaining the Very High–Very High combination as the highest level of concern. It therefore captures both areas already characterised by simultaneous upper-quintile conditions in the two hydroclimatic dimensions and areas where one or both indices occupy the adjacent High category. The resulting framework provides a comprehensive representation of the spatial extent and severity of hydroclimatic stress while maintaining a transparent and reproducible classification based on the historical climate distribution.

Although these extremes are not analysed as temporally concurrent compound events, their spatial coexistence reflects increasing hydroclimatic pressure under future climate conditions. Importantly, the combined-stress framework targets the upper tail of the hydroclimatic stress distribution and should not be interpreted as a full five-class composite index; by design, Classes 1–3 are excluded from the combined classification. The hydroclimatic stress identification framework is presented in Table 2.

**Table 2.** Hydroclimatic stress identification used in this study (Classification criteria and interpretation of the combined hydroclimatic stress levels based on the joint CDD and fraction of R95pTOT categories).

| Severity | Interpretation |
| --- | --- |
| Other | Areas characterised by both indices below High categories. |
| High | Areas characterised by high combined hydroclimatic stress, where both indicators reach at least the High category. These areas indicate substantial coexistence of prolonged dry conditions and a high proportional contribution of historically very wet days to annual precipitation. |
| Very High | Areas characterised by very high combined hydroclimatic stress, representing long uninterrupted dry conditions and a high proportional contribution of historically very wet days to annual precipitation. Priority areas for climate-risk governance and adaptation planning. |

### *2.5. Analysis, Visualisation and Watershed Aggregation*

All analyses and figures in this study were performed using MATLAB 2024a (The MathWorks, Inc., Natick, MA, USA), including data pre-processing, spatial averaging, and visualisation. Both absolute and percentage change maps were produced by comparing each future time slice against the historical baseline. The graphical abstract was created with the assistance of the generative AI tool ChatGPT--5.6 Sol (OpenAI), based on prompts and instructions provided by the authors. The graphical abstract is the only figure for which generative AI was used.

To evaluate regional-scale hydroclimatic stress patterns, the classified grid-cell results were spatially aggregated at the watershed level using the HydroBASINS Level 5 delineation. For each basin, the percentage of grid cells belonging to each hydroclimatic stress class was computed for every SSP and future period.

This procedure allowed the identification of spatial transitions in hydroclimatic stress conditions within major Iberian river basins and enabled inter-comparison between scenarios and future horizons. The watershed-scale aggregation also facilitates the interpretation of climate impacts within operational water-management units relevant for planning and adaptation.

## 3. Results

### *3.1. Changes in Mean Annual Precipitation*

The spatially averaged annual precipitation for 1991–2010 is approximately 700 mm, characterised by a well-defined southeast–northwest gradient. Higher precipitation values are observed in the northwestern quadrant (maximum around 1800 mm/year) and along orographically influenced regions such as the western Pyrenees (between 1200 and 1600 mm/year), while southeastern and interior areas remain significantly drier (under 600 mm/year) (see Figure A4). This historical precipitation distribution mainly reflects the influence of the Atlantic storm track and westerlies, with regional patterns shaped by topography and the transition toward Mediterranean climatic conditions.

The projections for the ensemble-mean annual precipitation (PR, mm/year) spatial patterns show under SSP1–2.6 a northwest–southeast rainfall gradient (Figure 2, top row). The Galician coast and the western Pyrenees are projected to sustain the highest totals (1600–1800 mm/year), while the southeastern interior remains semi-arid (300–400 mm/year). Slight drying conditions ($-50$ to $-100$ mm) are predicted to appear in southern Andalusia by 2081–2100, but overall changes remain within $\pm$ 10% of the 1991–2010 baseline.

Under SSP3–7.0, a moderate emissions scenario, the drying trends strengthen. By 2041–2060, precipitation in central Spain (Castile–La Mancha, Madrid) declines to 500–600 mm/year, and in southeastern zones to ~250 mm/year (Figure 2, middle row). The northern and northwestern regions experience modest decreases (<5%), reflecting a reduction in winter cyclonic activity. These drying patterns intensify by 2081–2100, with central Iberia falling below 400 mm/year. High emission forcing (SSP5–8.5) yields the most severe reductions in precipitation. In 2041–2060, PR in southern IP already falls below 350 mm/year, and by 2081–2100, totals dip below 300 mm/year in the central area (Figure 2, bottom row). Northern maxima decrease to 1500–1600 mm/year. The amplified contrasts underscore the vulnerability of inland and southern basins to intensifying aridity under unmitigated warming.

Figure 3 quantifies the spatial pattern of PR change (%) relative to the 1991–2010 baseline for the same scenarios and periods. A consistent feature across all scenarios is the progressive expansion and intensification of precipitation deficits with increasing radiative forcing and time. While early projections confine the largest reductions to southern Iberia,

the affected area gradually expands northwards in later periods, with both the magnitude and spatial extent of precipitation declines becoming increasingly pronounced under higher-emission scenarios. Under SSP1–2.6, projected changes remain modest (Figure 3, top row). During 2041–2060, most of the Peninsula exhibits near-neutral to slight negative anomalies, generally between 0 and −10%, with the largest reductions occurring over Andalusia and Murcia. By 2081–2100, drying becomes more evident in southern Iberia, where reductions locally approach −15%, while the Atlantic façade retains near-neutral or slightly positive changes (0 to +5%).

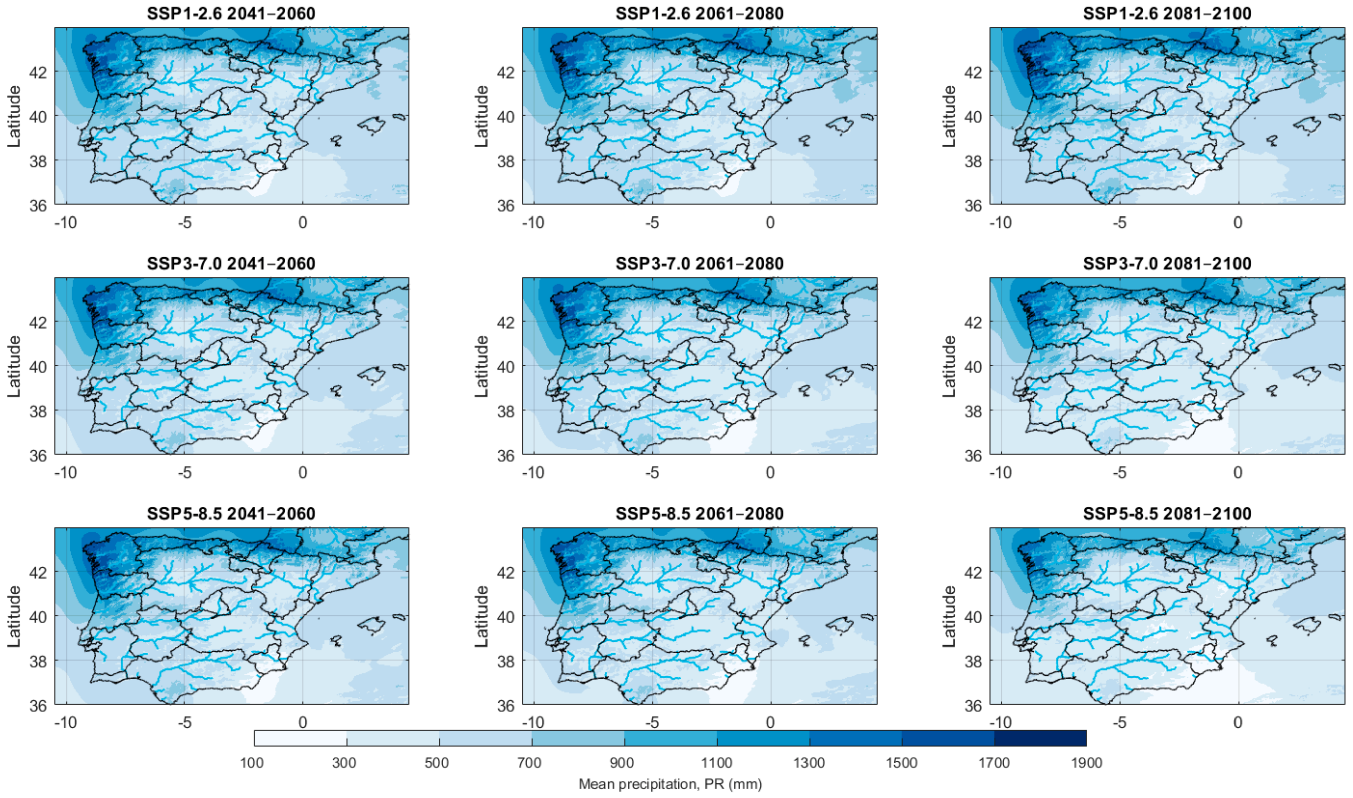



**Figure 2.** Projected annual mean precipitation (in mm) over the Iberian Peninsula under three Shared Socioeconomic Pathways (SSPs): SSP1–2.6 (**top** row), SSP3–7.0 (**middle** row), and SSP5–8.5 (**bottom** row). Each row shows projections for three future periods: 2041–2060 (**left**), 2061–2080 (**centre**), and 2081–2100 (**right**).

Under SSP3–7.0, drying becomes progressively more widespread (Figure 3, middle row). During 2041–2060, southern and central Iberia generally experience reductions between −5% and −15%. By 2061–2080, much of the interior exhibits decreases of approximately −10% to −15%, with locally larger reductions over southern Spain. By the end of the century, extensive areas of southern and central Iberia reach reductions between −15% and −25%, while northern regions generally remain between −5% and −10%.

The strongest drying occurs under SSP5–8.5 (Figure 3, bottom row). By 2041–2060, southern Iberia already exhibits reductions of approximately −10% to −20%. These drying trends intensify during 2061–2080, extending across much of central and southern Iberia with decreases commonly between −15% and −25%. By 2081–2100, extensive areas of the southern and interior Peninsula reach reductions approaching −25%, while locally larger decreases occur in the most affected regions. In contrast, northwestern Iberia remains comparatively less affected, with changes generally close to zero or only slightly negative.

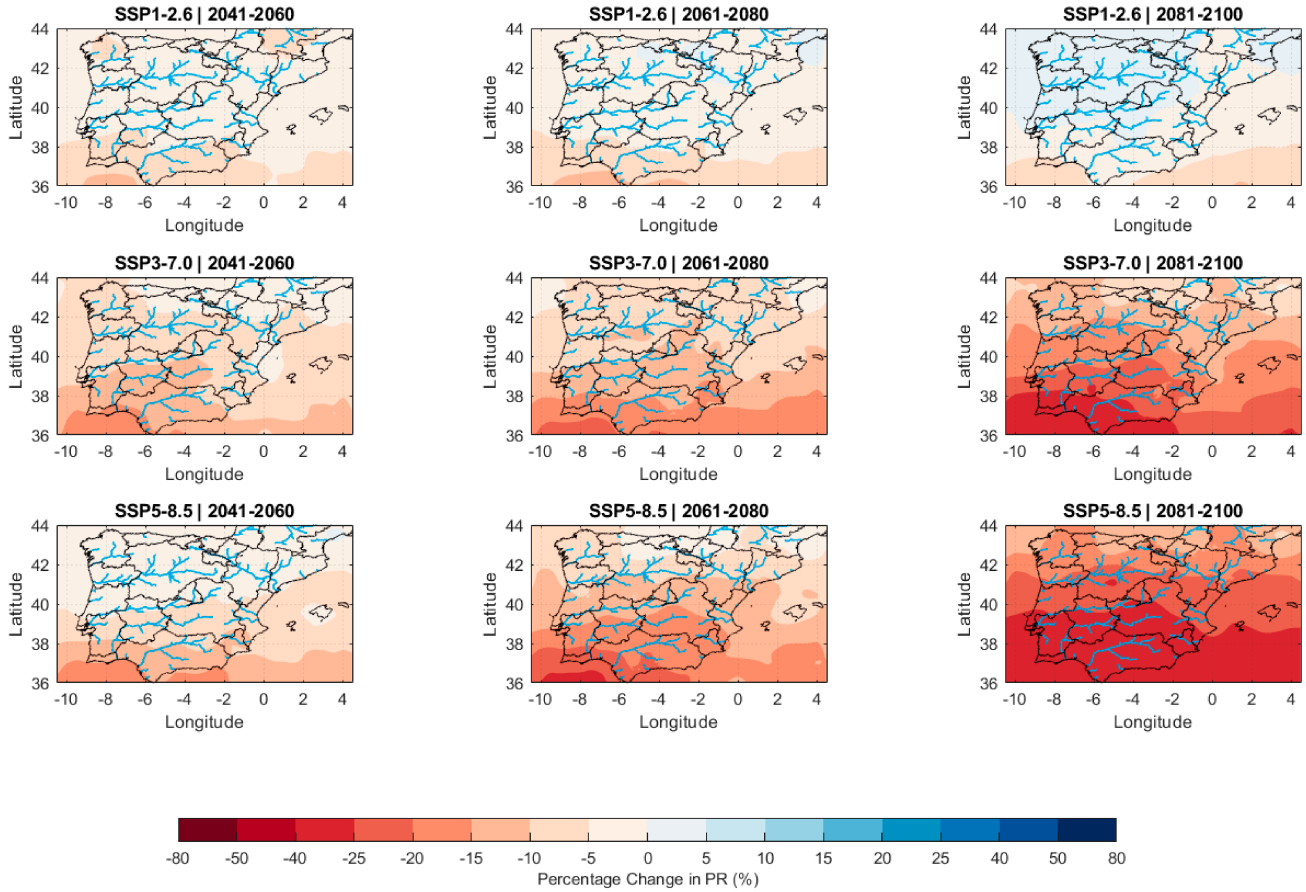



**Figure 3.** Spatial distribution of projected percentage change in total precipitation (PR) over the Iberian Peninsula relative to the historical baseline period (1991–2010). Rows correspond to different Shared Socioeconomic Pathways (SSPs): SSP1–2.6 (**top**), SSP3–7.0 (**middle**), and SSP5–8.5 (**bottom**). Columns indicate future time horizons: 2041–2060 (**left**), 2061–2080 (**centre**), and 2081–2100 (**right**). Positive values indicate an increase in precipitation, while negative values indicate a reduction.

### *3.2. Consecutive Dry Days (CDD)*

The spatial distribution of the annual maximum number of CDD during the historical period (1991–2010) shows a clear meridional gradient across the IP (Figure A5). The lowest CDD values are observed in the northwest (under 30 days/year), and the highest values exceed 60 days/year in the south, with the highest values in southern Andalusia. The higher CDD values observed across the southeastern and central interior regions are consistent with the semi-arid climate zones, while the lower CDD values observed in the northwest and along the Atlantic coast are associated with wetter climatic conditions.

In general, all scenarios indicate a progressive intensification and spatial expansion of prolonged dry conditions, with the strongest changes concentrated over southern and interior Iberia. Under SSP1–2.6, CDD increases remain comparatively moderate (Figure 4, top row). Southern and interior regions evolve from historical values of approximately 50–90 dry days/year to around 70–100 days/year by mid-century, reaching 90–110 days/year in Andalusia, Extremadura, and Castilla–La Mancha by 2081–2100. Atlantic-influenced sectors, including Galicia and the northwestern coastal regions, remain comparatively lower, generally below 40 days/year. Relative increases under this mitigation pathway remain mostly between +10% and +30% (Figure 5, top row), suggesting partial limitation of dry-condition intensification under lower greenhouse-gas forcing.

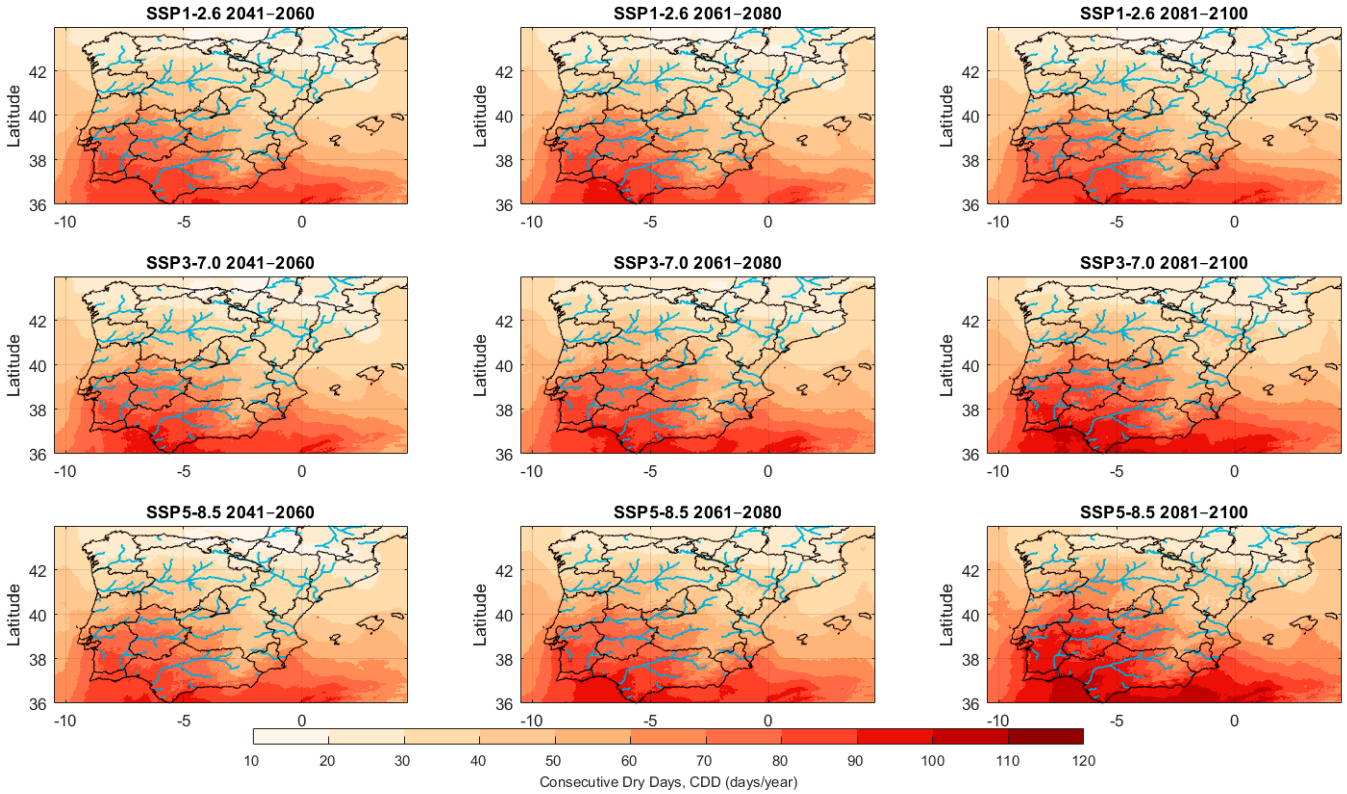



**Figure 4.** Spatial distribution of the mean number of consecutive dry days (CDD) over the Iberian Peninsula. Each row presents projections under three emission scenarios: SSP1–2.6 (**top** row), SSP3–7.0 (**middle** row), and SSP5–8.5 (**bottom** row), for the future periods 2041–2060, 2061–2080, and 2081–2100. The colour scale, consistent across all panels, ranges from light yellow (fewer dry days) to deep red (more dry days), highlighting an increase in the duration of the longest annual dry spell.

In contrast, SSP3–7.0 and SSP5–8.5 produce a marked amplification of dry conditions across the Peninsula (Figure 4, middle and bottom rows). Under SSP3–7.0, southern Iberia progressively reaches 70–110 consecutive dry days per year by 2061–2080, while large sectors of central and southern Spain exceed 80 dry days annually by the end of the century. Northern and Atlantic regions also experience substantial increases, with CDD values commonly reaching 40–50 days/year. Under SSP5–8.5, the intensification becomes particularly clear, with inland and southern basins exceeding 70–90 days/year by mid-century and surpassing 90 consecutive dry days/year in parts of the Guadiana and Guadalquivir basins by 2081–2100.

The relative changes shown in Figure 5 reinforce the progressive acceleration of dry conditions under stronger forcing scenarios. SSP3–7.0 yields an increase of approximately +25% to +40% across central and southern Iberia by mid-century, locally exceeding +50% by 2081–2100. Under SSP5–8.5, projected increases become particularly pronounced in southern and interior watersheds, where late-century relative increases in CDD frequently exceed +60% to +80%. Even northern sectors exhibit increases of +30% to +40%, indicating that prolonged dry conditions may become increasingly widespread across the entire Peninsula under high-emission trajectories. Across all emission scenarios, the area affected by longer consecutive dry periods progressively expands from southern and southeastern Iberia to the central and northern regions. This expansion becomes increasingly pronounced with both time and radiative forcing, indicating that dry conditions are projected to intensify over progressively larger portions of the Peninsula. These projections indicate that future hydroclimatic conditions across Iberia may increasingly favour extended, potentially multi-

month uninterrupted dry periods, particularly in regions already characterised by structural water stress.

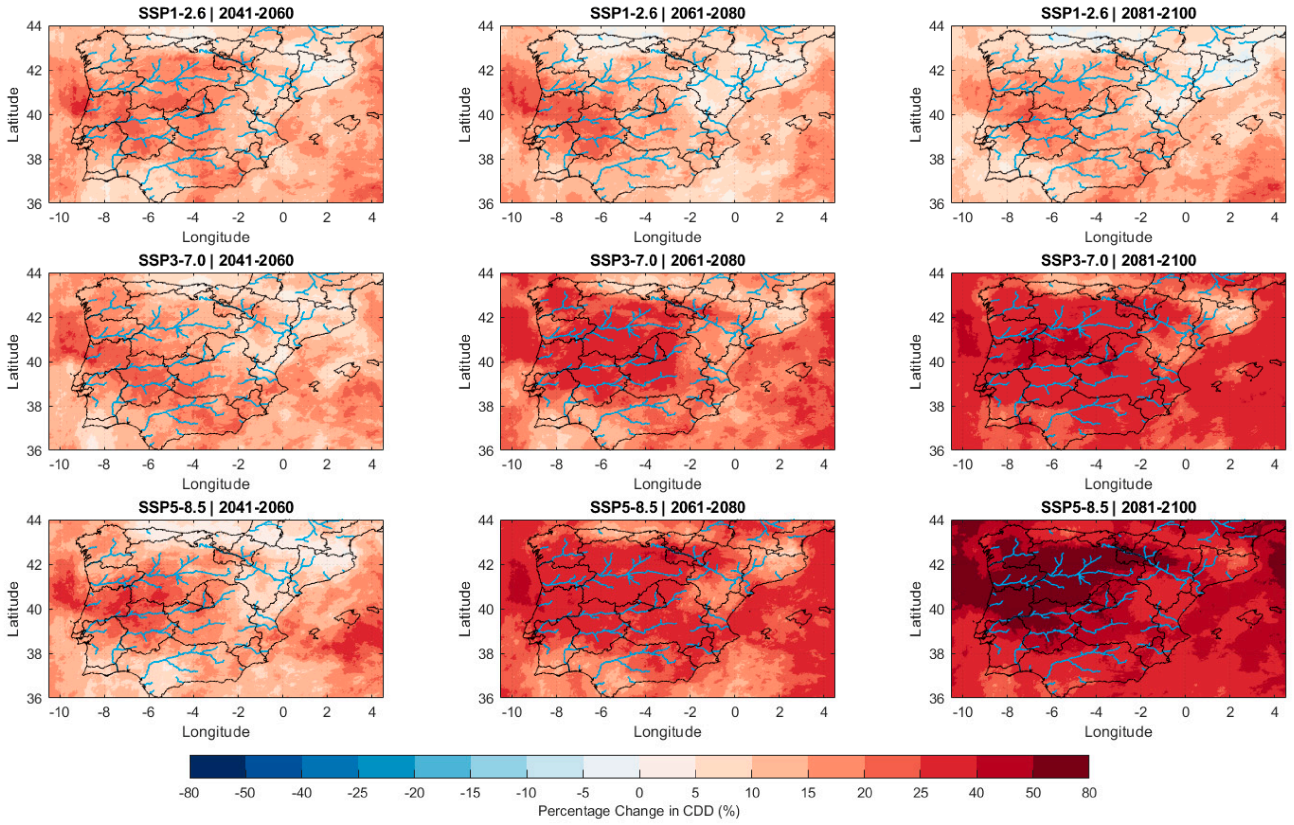



**Figure 5.** Spatial distribution of projected percentage change in consecutive dry days (CDD) over the Iberian Peninsula relative to the historical baseline period (1991–2010). Rows correspond to different Shared Socioeconomic Pathways (SSPs): SSP1–2.6 (**top**), SSP3–7.0 (**middle**), and SSP5–8.5 (**bottom**). Columns indicate future time horizons: 2041–2060 (**left**), 2061–2080 (**centre**), and 2081–2100 (**right**). Positive values indicate an increase in dry spell duration, while negative values indicate a reduction. The colour scale is consistent across all subplots to enable direct comparison.

### *3.3. Number of Dry Spells (CDDn)*

Figure A6 presents the spatial distribution of the annual mean number of CDD periods exceeding five days, i.e., dry spells, for the historical baseline (1991–2010). This metric is particularly relevant for characterising dry-spell fragmentation, namely the frequency with which dry periods recur throughout the year, rather than their duration alone. However, changes in CDDn should not be interpreted in isolation. A reduction in the number of dry spells may indicate either fewer dry-spell episodes or the occurrence of longer dry periods resulting from the merging of shorter events. For this reason, CDDn is analysed jointly with CDD, allowing changes in both the frequency and maximum duration of uninterrupted dry conditions to be distinguished. In the historical reference period, most of the IP experienced between 10 and 18 dry periods per year, with relatively higher frequencies in the northeastern and interior regions (Figure A6). The northwest, including parts of Galicia and northern Portugal, displayed the lowest CDDn values, generally below 13 dry spells per year, consistent with their more maritime climate. Values below 12 dry spells per year are also observed in the southernmost regions of Portugal and Andalusia in Spain.

Overall, the projections indicate a progressive expansion of regions experiencing more frequent dry spells across the Peninsula when compared with the historical baseline, with

the strongest increases concentrated over eastern and northeastern Iberia. When interpreted together with CDD, these changes reflect evolving patterns of dry-spell fragmentation under future climate conditions. Under SSP1–2.6, increases in CDDn remain comparatively moderate (Figure 6, top row). Northeastern and interior sectors (Aragón, Cataluña and Comunidad Valenciana) increase to more than 15 events per year across northeastern and Mediterranean-facing regions by the end of the century. At the same time, Atlantic-influenced and mountainous regions display only limited changes. Relative increases generally remain below +30% across most of the Peninsula (Figure 7, top row), highlighting the moderating influence of sustained climate mitigation.

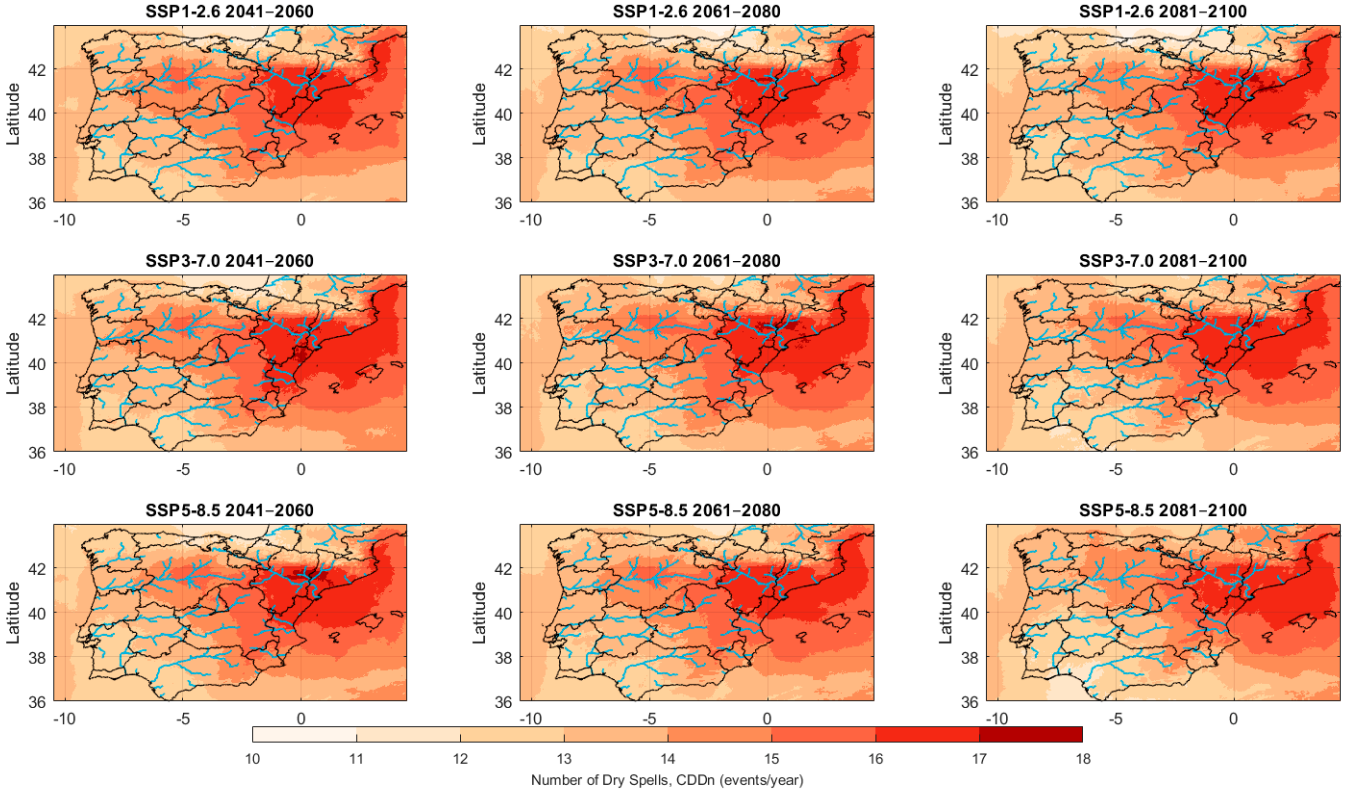



**Figure 6.** Spatial distribution of the mean number of dry spells (CDDn) over the Iberian Peninsula. Each row presents projections under three emission scenarios: SSP1–2.6 (**top** row), SSP3–7.0 (**middle** row), and SSP5–8.5 (**bottom** row), for the future periods 2041–2060, 2061–2080, and 2081–2100. The colour scale, consistent across all panels, ranges from light yellow (fewer dry spells) to deep red (more dry spells), highlighting increases in dry-spell recurrence.

Under SSP3–7.0 and SSP5–8.5, the spatial pattern of CDDn becomes increasingly heterogeneous (Figure 6, middle and bottom rows). Northeastern and eastern Iberia experience a progressive expansion of areas with more frequent dry spells, with values of approximately 16–18 dry spells per year becoming increasingly widespread across northeastern Iberia and the Mediterranean domain by the end of the century. Parts of southern and southwestern Iberia show little change or even slight reductions in CDDn. These contrasting responses are also evident in the relative change maps (Figure 7), where positive changes are concentrated over eastern and northeastern regions, whereas locally negative or near-neutral changes occur in the south.

The contrasting spatial responses suggest that climate change will not modify dry-spell characteristics uniformly across the IP. Instead, eastern regions are projected to experience more frequent dry-spell occurrences, whereas southern regions tend towards fewer but

longer dry episodes, highlighting the importance of jointly analysing CDD and CDDn to distinguish changes in dry conditions from changes in dry-spell fragmentation.

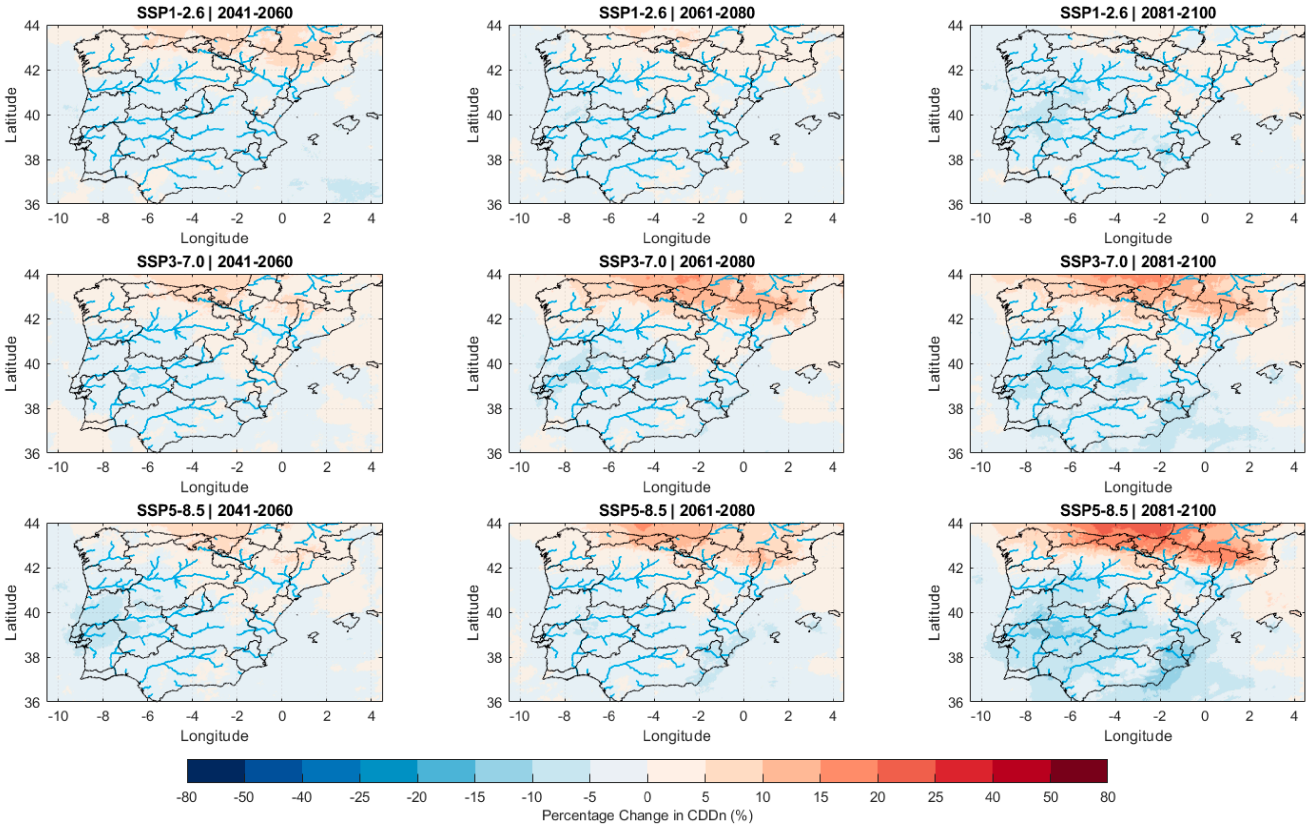



**Figure 7.** Percentage change in the mean number of dry spells (CDDn) relative to the historical period (1991–2010) under three Shared Socioeconomic Pathways (SSPs): SSP1–2.6 (**top** row), SSP3–7.0 (**middle** row), and SSP5–8.5 (**bottom** row). Each row displays changes for three future time slices: 2041–2060, 2061–2080, and 2081–2100. Blue shades indicate projected decreases in dry-spell recurrence, while red shades represent increases. The colour scale is consistent across all panels (−80% to +80%) to allow direct comparison among scenarios and timeframes.

### *3.4. Fraction of Precipitation from Very Wet Days (R95pTOT)*

The historical spatial distribution of the fraction of R95pTOT over the IP reveals a pronounced northwestern-to-southeastern gradient in precipitation concentration (Figure A7). Expressed as a percentage, R95pTOT represents the fraction of total annual precipitation accumulated during very wet days exceeding the historical 95th percentile threshold. Higher values, therefore, indicate that a larger proportion of annual precipitation is concentrated into a limited number of intense precipitation events.

The highest fraction of R95pTOT values is observed across southeastern and Mediterranean Iberia, particularly along the Mediterranean coast, southeastern Spain, and parts of eastern Andalusia, where values frequently exceed 40–60% of annual precipitation totals. These high percentages hint at irregular rainfall regimes in which a substantial fraction of annual precipitation occurs on days exceeding the historical 95th-percentile threshold. Such conditions are characteristic of Mediterranean climates, where convective storms and episodic heavy precipitation contribute disproportionately to annual rainfall totals.

Conversely, the northwestern Atlantic-influenced regions, including Galicia, the Cantabrian coast, and the western Pyrenees, exhibit the lowest fraction of R95pTOT values, generally below 30% (Figure A7). These lower percentages reflect more evenly distributed precipitation regimes associated with the frequent passage of Atlantic frontal systems,

which deliver rainfall more regularly throughout the year rather than concentrating precipitation into isolated extreme events. Intermediate values (around 30–40%) are observed across central Iberia and along major mountain systems, where topographic effects locally influence the contribution of very wet days to annual precipitation, while maintaining a relatively mixed rainfall regime.

The projections indicate the persistence of the historical northwestern-to-southeastern gradient in precipitation concentration, with the highest fraction of R95pTOT values consistently observed over southeastern and Mediterranean Iberia and the lowest values over the Atlantic-influenced northwestern regions (Figure 8). Under SSP1–2.6, projected changes remain relatively moderate throughout the century (Figure 8, top row). The spatial distribution indicates that the areas with the fraction of R95pTOT exceeding 45–55% will expand slightly inland across eastern and southeastern Iberia. In contrast, Galicia, the Cantabrian coast, and the western Pyrenees continue to exhibit the lowest values, generally below 40%, reflecting the persistence of more evenly distributed Atlantic precipitation regimes. This projected increase in the fraction of very wet days underscores a fundamental shift toward more concentrated precipitation regimes, particularly under unmitigated warming in the southeastern regions of the IP.

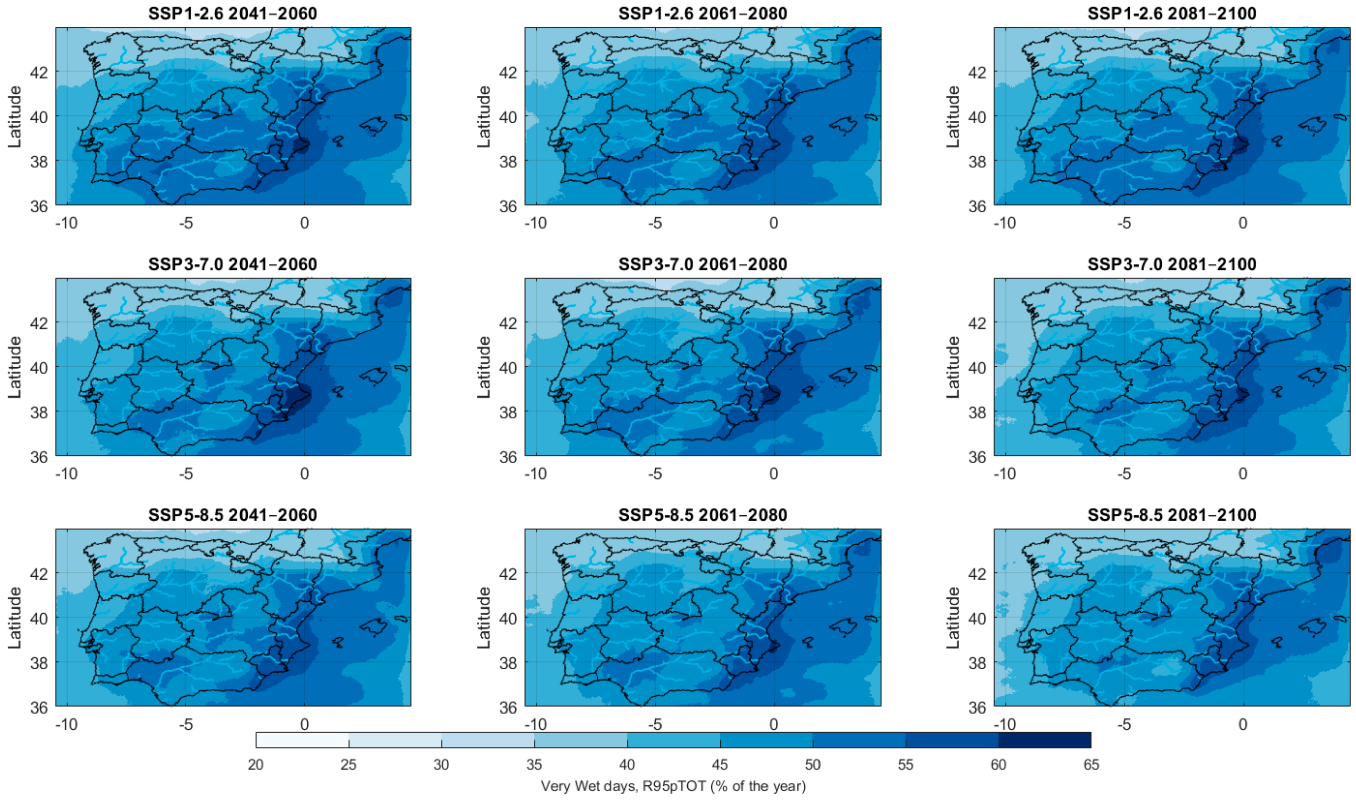



**Figure 8.** Spatial distribution of the mean fraction of annual precipitation occurring on very wet days (R95pTOT) over the Iberian Peninsula. Each row presents projections under three emission scenarios: SSP1–2.6 (**top** row), SSP3–7.0 (**middle** row), and SSP5–8.5 (**bottom** row), for the future periods 2041–2060, 2061–2080, and 2081–2100. The colour scale ranges from light blue, indicating a smaller contribution of very wet days to annual precipitation, to deep blue, indicating a larger contribution.

Under SSP3–7.0, a higher fraction of R95pTOT values will be widespread across eastern and southeastern Iberia, with extensive areas exceeding 45% by the late century (Figure 8, middle row). Values above 60% remain largely confined to the Mediterranean coastal belt and adjacent regions, though the maximum values are depicted for 2041–2060. This points to more than half of the annual precipitation being projected to occur on

days exceeding the historical 95th-percentile threshold. The Atlantic northwestern regions continue to maintain lower values, generally below 40%, although slight increases relative to the historical baseline become apparent.

Under SSP5–8.5 (Figure 8, bottom row), high fractional R95pTOT values occur across eastern, southeastern and parts of central Iberia, while the Mediterranean coastal belt continues to exhibit the largest fractions of annual precipitation (> 50%) occurring during very wet days. Such values imply that more than half of the total annual precipitation may be delivered during a limited number of very wet days, representing an increase in rainfall concentration and hydroclimatic irregularity.

The percentage-change maps (Figure 9) reveal a remarkably consistent spatial pattern across all emission scenarios during the mid-century period (2041–2060). A distinct northeast–southwest-oriented transition separates the northern half of the IP, where increases in the fraction of R95pTOT generally range between 20% and 40%, from the southern regions, where projected changes are predominantly below 15%. Galicia constitutes a notable exception, exhibiting comparatively moderate increases of approximately 15–25%. Towards the end of the century (Figure 9, third column), this spatial pattern evolves progressively with increasing radiative forcing.

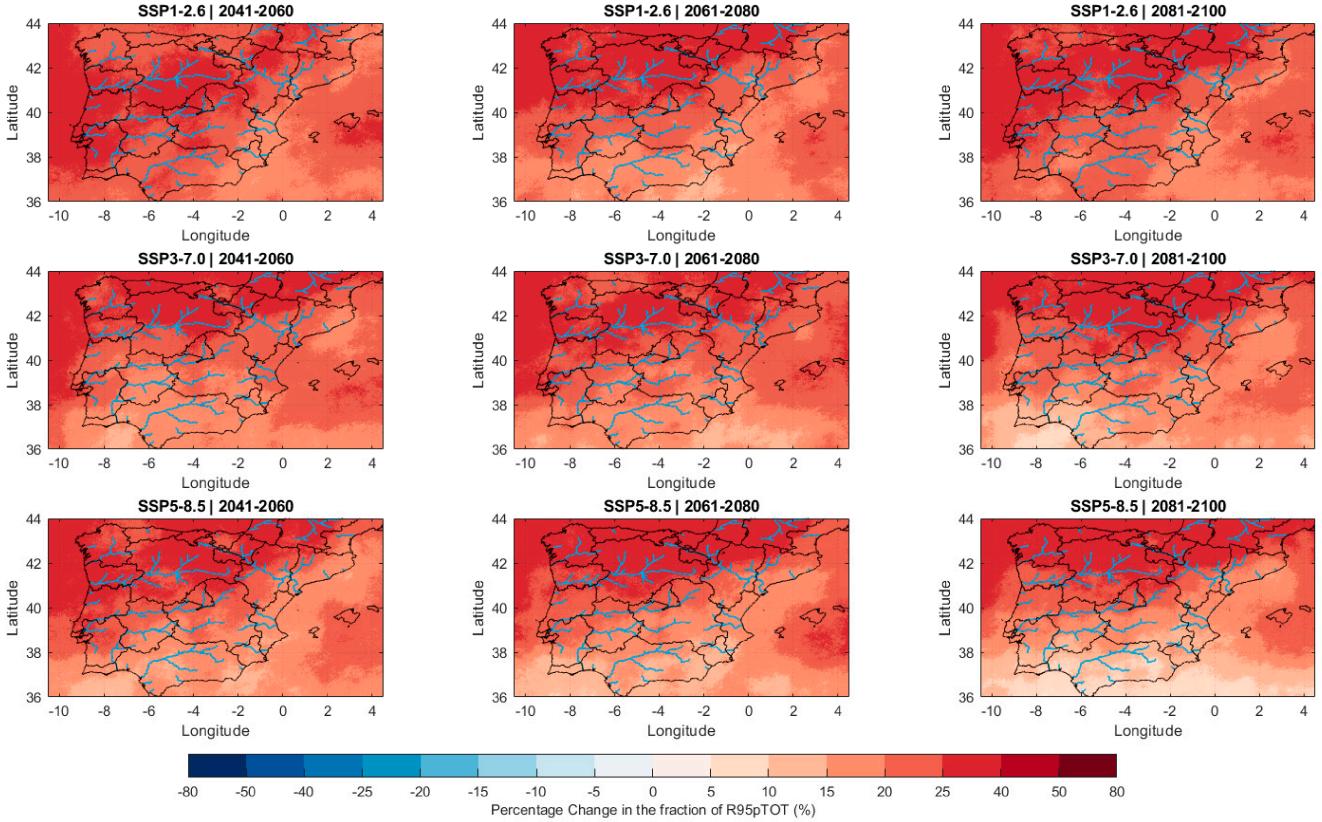



**Figure 9.** Percentage change in the mean percentage of very wet days (R95pTOT) relative to the historical period (1991–2010) under three Shared Socioeconomic Pathways (SSPs): SSP1–2.6 (**top** row), SSP3–7.0 (**middle** row), and SSP5–8.5 (**bottom** row). Each row displays changes for three future time slices: 2041–2060, 2061–2080, and 2081–2100. Blue shades indicate projected decreases in the percentage of very wet days, while red shades represent increases. The colour scale is consistent across all panels (−80% to +80%) to allow direct comparison among scenarios and timeframes.

The region of larger percentage changes expands westwards to include Galicia, where increases reach 25–40% commonly, while the area characterised by relatively modest changes (<15%) extends northwards across parts of the interior and along the Mediter-

ranean coast. This redistribution becomes increasingly pronounced under SSP5–8.5, highlighting an enhanced spatial contrast in the projected concentration of annual precipitation into relatively few very wet days. These changes indicate progressively more irregular precipitation regimes characterised by extended dry conditions and a growing concentration of annual precipitation on very wet days.

### *3.5. Hydroclimatic Stress Patterns Under Future Climate Scenarios*

#### 3.5.1. Basin-Scale Evolution of PR and CDDn

To complement the spatial analyses, the historical quintile thresholds were applied to PR and CDDn at the watershed scale (Figures 10 and 11). Although these variables are not directly incorporated into the hydroclimatic stress framework, their basin-scale distributions provide additional insight into the evolution of precipitation availability and dry-spell fragmentation across the principal Iberian river basins.

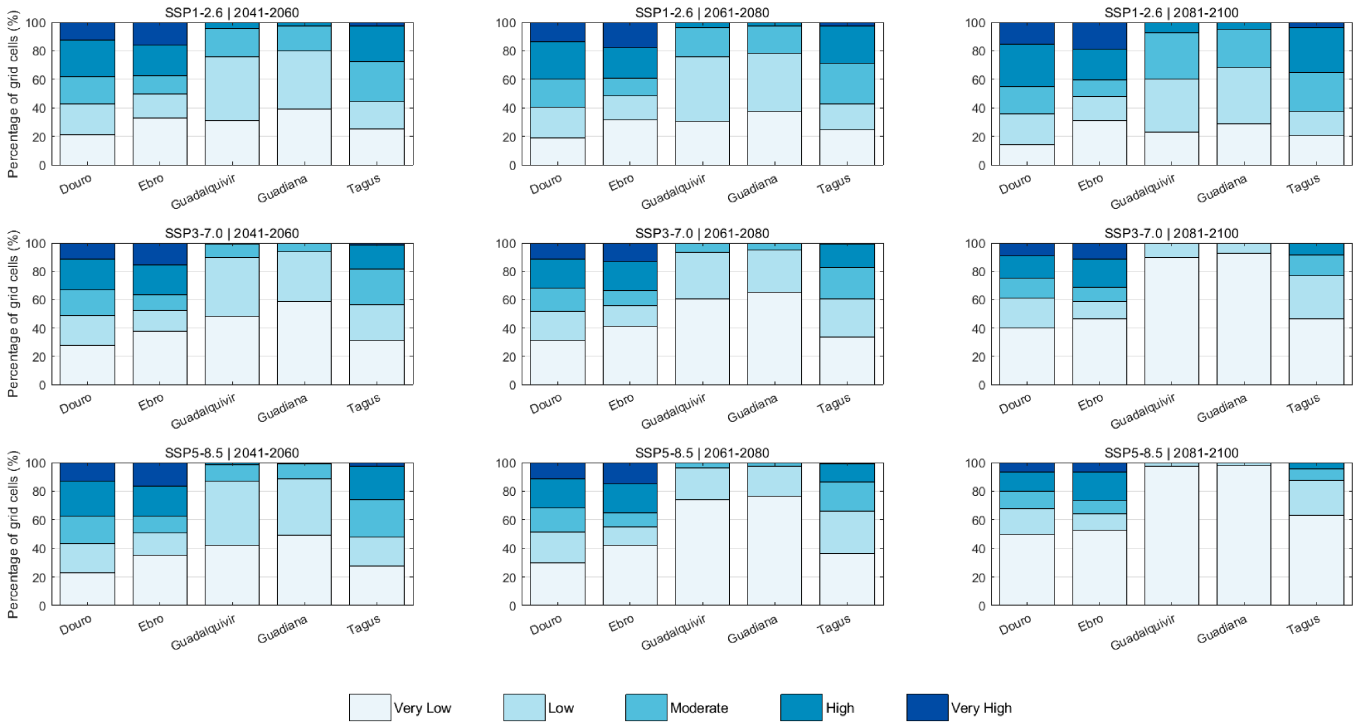



**Figure 10.** Percentage of watershed grid cells belonging to each PR quintile class for major Iberian river basins under SSP1–2.6 (**top** row), SSP3–7.0 (**middle** row), and SSP5–8.5 (**bottom** row), for the periods 2041–2060, 2061–2080, and 2081–2100. The classes were obtained from the PR quintiles relative to the historical baseline (1991–2010).

The watershed-scale quintile distributions of PR reinforce the spatial patterns discussed previously (see Section 3.1) by highlighting the progressive redistribution of precipitation classes across the main Iberian river basins. During the historical baseline (1991–2010), the Douro and Ebro basins exhibit the largest proportions of the "High" and "Very High" precipitation classes, reflecting the wetter climatic conditions of northern Iberia, whereas the Guadalquivir, Guadiana and Tagus basins are characterised by a greater prevalence of the "Very Low", "Low" and "Moderate" classes. Future projections indicate a gradual shift towards the lower precipitation quintiles, with the major changes occurring under SSP5–8.5 by the end of the century (Figure 10). This transition is particularly evident in the Guadalquivir and Guadiana basins, where the "Very Low" and "Low" classes become increasingly dominant, while the Tagus basin exhibits a similar, although less pronounced, tendency. Although the Douro and Ebro basins remain comparatively wetter throughout

the projection period, both experience a progressive reduction in the "High" and "Very High" precipitation classes, indicating a basin-wide redistribution towards drier historical conditions under increasing radiative forcing (Figure 9, bottom row).

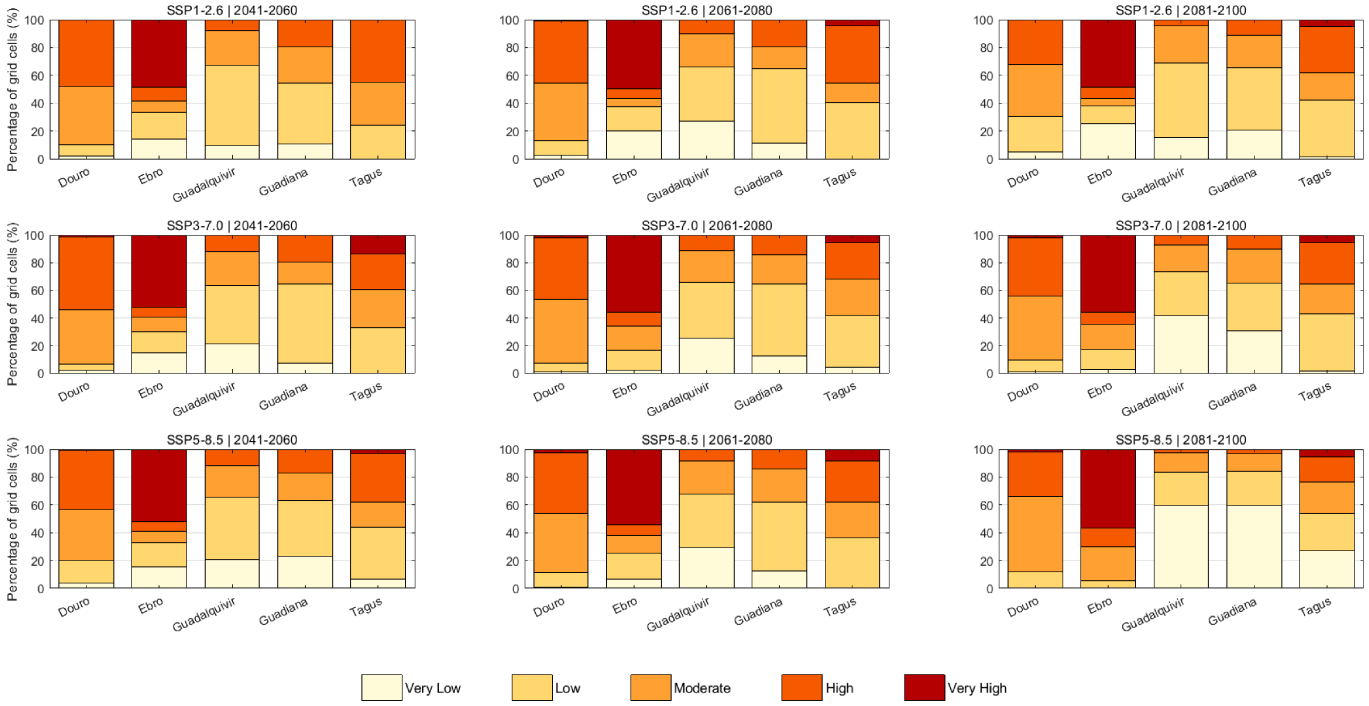



**Figure 11.** Percentage of watershed grid cells belonging to each CDDn quintile class for major Iberian river basins under SSP1–2.6 (**top** row), SSP3–7.0 (**middle** row), and SSP5–8.5 (**bottom** row), for the periods 2041–2060, 2061–2080, and 2081–2100. The classes were obtained from the CDDn quintiles relative to the historical baseline (1991–2010).

The watershed-scale quintile distributions of CDDn (Figure 11) complement the spatial analysis (see Section 3.3) by illustrating how the frequency of consecutive dry periods evolves across the principal Iberian river basins. During the historical baseline (1991–2010), the Ebro basin exhibits the largest proportion of the "Very High" CDDn class, while the Douro and Tagus are predominantly characterised by the "High" class, reflecting the greater occurrence of dry-spell events in northern and northeastern Iberia. In contrast, the Guadalquivir and Guadiana basins display larger proportions of the "Very Low" and "Low" classes, indicating fewer dry-spell occurrences under the historical climate. Future projections indicate relatively modest changes compared with PR, although a gradual redistribution towards the lower CDDn quintiles is evident in the southern basins, particularly under SSP5–8.5 by the end of the century (Figure 11, bottom row).

This tendency is most pronounced in the Guadalquivir and Guadiana basins, while the Tagus also exhibits an increasing prevalence of the "Very Low" and "Low" classes. Conversely, the Ebro basin consistently retains the highest proportion of the "Very High" class throughout the projection period. These basin-scale changes reinforce the spatial analysis by indicating a transition towards fewer dry-spell events in southern Iberia, consistent with the simultaneous increase in CDD and suggesting an evolution towards fewer, but more extended dry periods.

### 3.5.2. Basin-Scale Evolution of CDD and the Fraction of R95pTOT

The projections for the spatial distribution of the five CDD quintile classes across the IP show a persistent latitudinal organisation for the historical period (Figure A8a), as well as for all projections (Figure A9). The "Very High" class consistently occupies the

southernmost regions of the Peninsula, particularly across the Guadiana, Guadalquivir and Tagus river basins. The projected expansion towards the north of this class in comparison with 1991–2010 is noteworthy. In contrast, the most noticeable changes occur in northern Iberia, where the spatial extent of the "Very Low" class progressively contracts with increasing radiative forcing and time, becoming considerably more restricted by the end of the century under SSP5–8.5 (Figure A9, bottom row). Simultaneously, northeastern Iberia exhibits a gradual transition from the "Moderate" to the "High" class, indicating an expansion of longer consecutive dry periods into regions that historically experienced less extended dry conditions. These changes are also reflected at the watershed scale, particularly within the Douro and Ebro river basins, where the northward expansion of higher CDD classes becomes increasingly evident. Overall, although the broad latitudinal distribution of CDD remains largely unchanged, the progressive contraction of the lowest classes and the expansion of higher classes indicate a widespread intensification of dry conditions under future climate change, particularly under the high-emission scenario.

During the historical baseline (Figure A8b), the "Very High" class for the fraction of R95pTOT quintiles was largely confined to the Mediterranean coast, particularly along the eastern seaboard, and to western Andalusia, whereas most of the interior of the IP was characterised by lower quintile classes. Overall, the broad spatial distribution remains relatively stable, with the "Very High" class continuing to dominate much of the Mediterranean and southern Iberian regions. Consequently, differences among scenarios are mainly expressed through local transitions from the "Very High" to the "High" class rather than widespread redistribution among all quintile classes. These transitions occur predominantly in Portugal, where the reduction in stress class progressively extends from north to south along the Atlantic coast. Under SSP1–2.6, this shift remains largely confined to northern Portugal (Figure A10, top row), whereas under SSP3–7.0 it gradually expands southwards (Figure A10, middle row). The most pronounced changes are projected under SSP5–8.5 by the end of the century (2081–2100), when "High" stress conditions extend along much of the Portuguese Atlantic coast, reaching southern Portugal (Figure A10, bottom row). In contrast, future projections indicate a marked expansion of the "Very High" class across the interior of the Peninsula, progressively extending from the Mediterranean domain to the southern interior under increasing radiative forcing. At the watershed scale, this expansion encompasses most of the major river basins of southern Iberia, particularly the Guadiana, Guadalquivir, Júcar, Segura and Ebro basins. In contrast, the transition from the "Very High" to the "High" class along the Portuguese Atlantic coast is mainly reflected in the Douro, Mondego (entirely Portuguese) and Tagus river basins.

The watershed-scale quintile distributions of CDD (Figure 12) reinforce the spatial analysis (see Section 3.2) by illustrating how dry conditions evolve across the principal Iberian river basins. During the historical baseline (1991–2010), the Douro and Ebro basins are dominated by the "Very Low", "Low" and "Moderate" CDD classes, reflecting the shorter consecutive dry periods characteristic of northern Iberia, whereas the Guadalquivir and Guadiana basins exhibit a predominance of the "High" and "Very High" classes. The Tagus basin displays an intermediate behaviour, with a substantial proportion of grid cells already classified within the "High" class under historical conditions (Figure A8a). Future projections indicate a progressive redistribution towards the upper CDD quintiles across all basins, with the most pronounced changes occurring under SSP5–8.5 by the end of the century (Figure 12, bottom row). This transition is particularly evident in the Douro and Ebro basins, where the "Very Low" and "Low" classes progressively contract while the "Moderate" and "High" classes become increasingly dominant. Although the Guadalquivir and Guadiana basins remain characterised by the highest dry spell classes throughout the projection period, the expansion of the "High" and "Very High" classes

into the northern basins demonstrates that longer consecutive dry periods are projected to affect progressively larger portions of the IP under increasing radiative forcing.

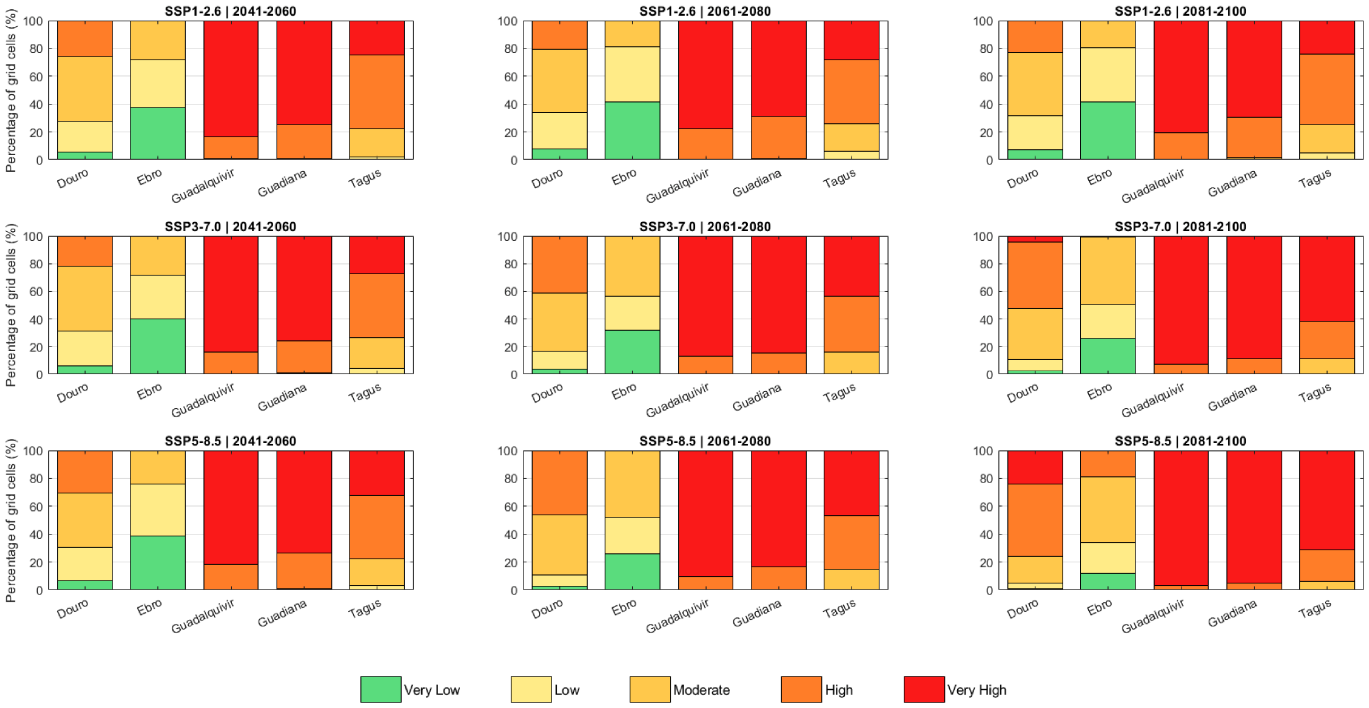



**Figure 12.** Percentage of watershed grid cells belonging to each CDD quintile class for major Iberian river basins under SSP1–2.6 (**top** row), SSP3–7.0 (**middle** row), and SSP5–8.5 (**bottom** row), for the periods 2041–2060, 2061–2080, and 2081–2100. Stress classes were obtained from the classification relative to the historical CDD baseline (1991–2010) (Figure related to Table A2).

During the historical baseline (1991–2010), the "Very High" quintile class distribution of the fraction of R95pTOT is predominantly confined to the Mediterranean-influenced basins, particularly the Júcar, Segura and Ebro, while the Atlantic-influenced Douro basin is characterised by a greater proportion of the "Low" and "Moderate" classes. Future projections indicate progressive redistribution towards the upper R95pTOT quintiles, reflecting an increasing concentration of annual precipitation into relatively few very wet days (Figure 13). This transition becomes increasingly evident under SSP3–7.0 and SSP5–8.5, when the "Very High" class expands across the southern and interior basins, particularly the Guadiana, Guadalquivir and Tagus, while remaining dominant in the Mediterranean basins. In contrast, the Douro basin continues to exhibit a larger proportion of the "High" class, although the "Very High" category also becomes increasingly represented towards the end of the century. Overall, the basin-scale classifications indicate that progressively larger fractions of the major Iberian river basins are projected to experience precipitation regimes characterised by a stronger concentration of annual rainfall on very wet days, particularly under higher-emission scenarios (Figure 13, bottom row).

Taken together, the CDD and fractional R95pTOT classifications reveal that the projected hydroclimatic evolution is not spatially uniform across the Iberian basins. Southern and interior basins increasingly combine already elevated CDD conditions with an expansion of the upper R95pTOT classes, whereas northern and Atlantic-influenced basins show a more progressive transition from historically lower dry-period classes. This contrast indicates that future hydroclimatic change involves both an intensification of existing south–north gradients and their progressive extension into basins that historically experienced less severe dry conditions.

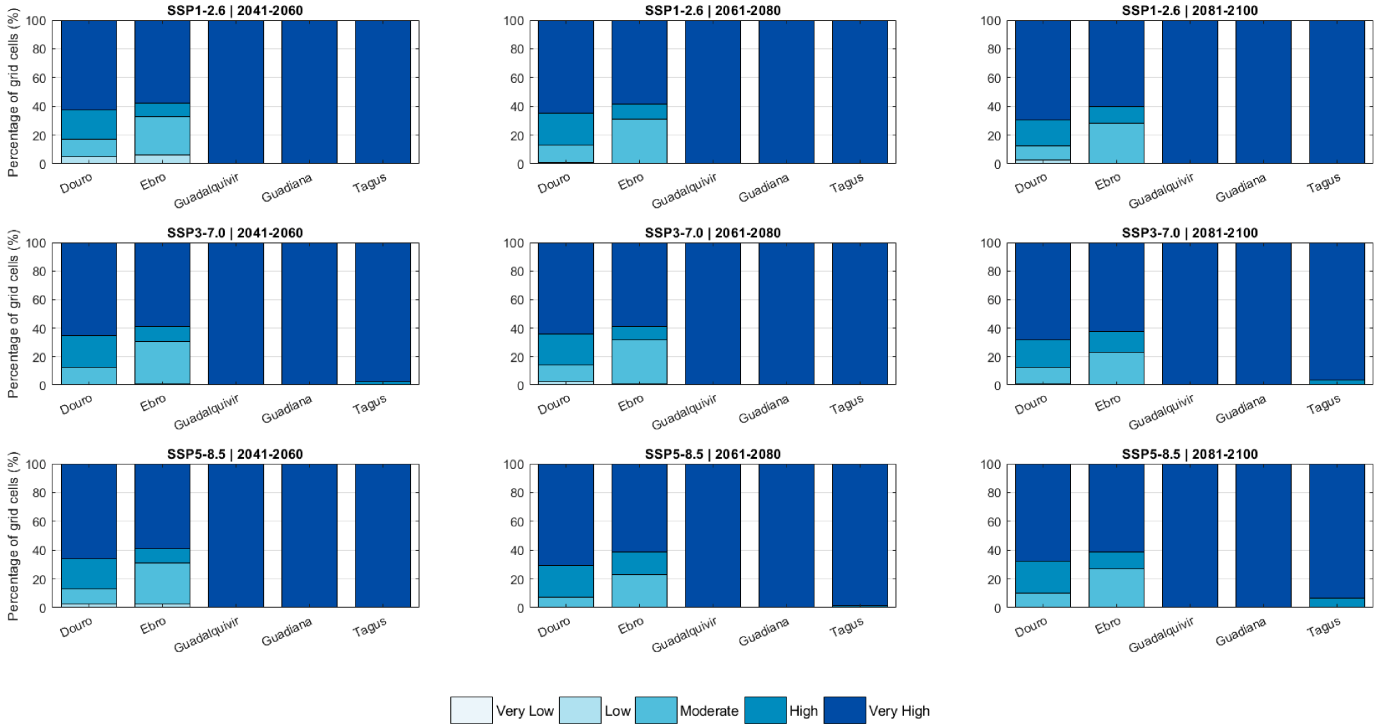



**Figure 13.** Percentage of watershed grid cells belonging to each R95pTOT quintile class for major Iberian river basins under SSP1–2.6 (**top** row), SSP3–7.0 (**middle** row), and SSP5–8.5 (**bottom** row), for the periods 2041–2060, 2061–2080, and 2081–2100. Stress classes were obtained from the fraction of R95pTOT classification relative to the historical fraction of R95pTOT baseline (1991–2010). (Figure related to Table A3).

### 3.5.3. Combined Hydroclimatic Stress Framework

The spatial distribution of combined hydroclimatic stress (Figures A8c and A11) reveals a progressive expansion of both "High" and "Very High" stress conditions with increasing radiative forcing and time. During the historical baseline, "Very High" hydroclimatic stress is largely confined to limited sectors of southern and Mediterranean Iberia, while the "High" category delineates a broader transitional zone surrounding these core stress areas. Future projections indicate an expansion of both categories towards the interior and progressively farther north, with the largest spatial extent occurring under SSP5–8.5 by the end of the century (Figure A11, bottom row). "Very High" stress remains most persistent across southern Iberia, particularly within the Guadalquivir, Guadiana and Tagus regions, whereas the "High" category identifies a broader geographical domain in which elevated dry-period persistence and precipitation concentration increasingly coexist.

The watershed-scale distributions (Figure 14) reinforce these spatial patterns by quantifying the proportions of each basin classified as "High" and "Very High" hydroclimatic stress. The Guadalquivir and Guadiana basins exhibit the greatest exposure, with "Very High" stress already accounting for a large proportion of their area and becoming increasingly dominant under stronger radiative forcing and towards the end of the century. The Tagus displays a more progressive transition, with substantial areas initially classified as "High" stress shifting towards the "Very High" category, particularly under SSP3–7.0 and SSP5–8.5. In contrast, the Douro remains predominantly outside the "High" and "Very High" stress categories, while the Ebro shows comparatively limited exposure. These basin-scale patterns indicate that future hydroclimatic change involves both the expansion of elevated combined stress and, particularly in the southern and interior basins, a transition from "High" to "Very High" stress conditions.

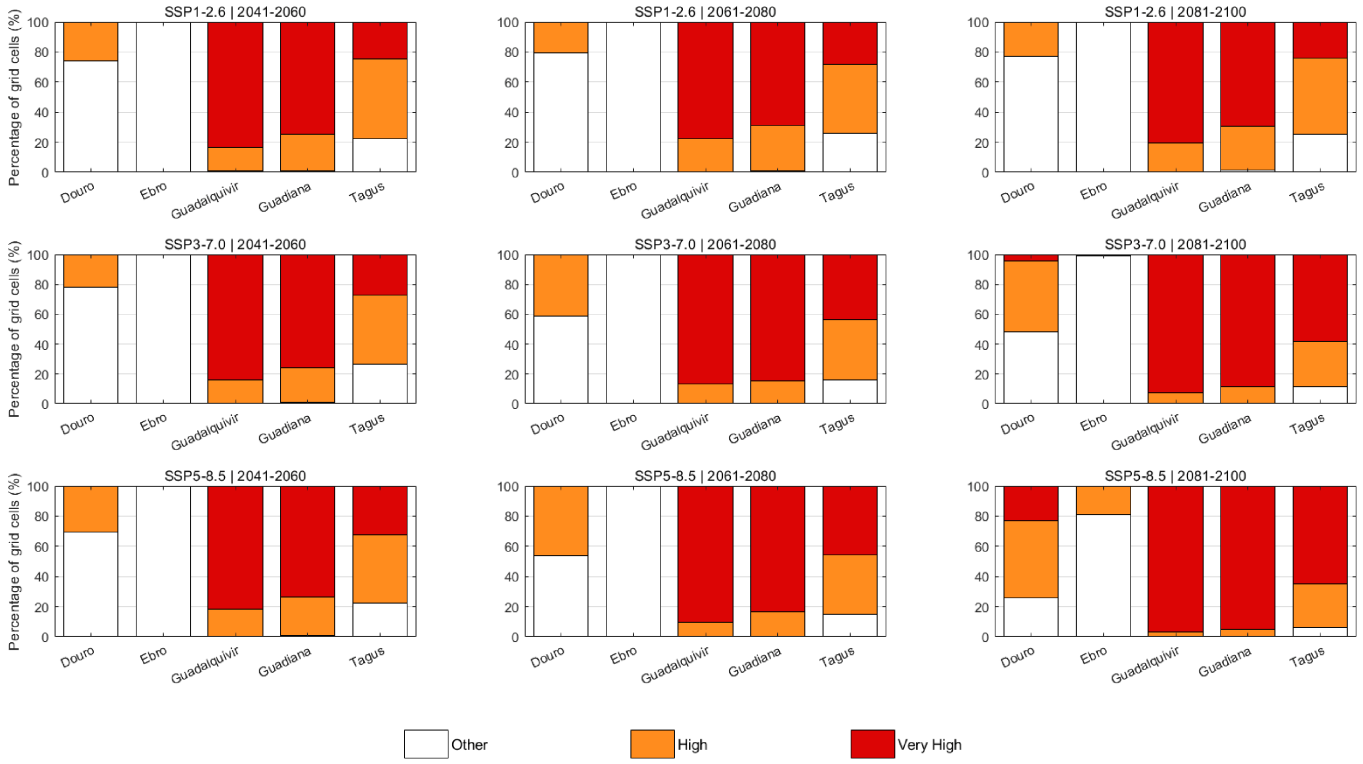



**Figure 14.** Percentage of watershed grid cells classified as Other, High, and Very High hydroclimatic stress for major Iberian river basins under SSP1–2.6 (**top** row), SSP3–7.0 (**middle** row), and SSP5–8.5 (**bottom** row), for the periods 2041–2060, 2061–2080, and 2081–2100. High hydroclimatic stress comprises grid cells with CDD–fraction of R95pTOT quintile combinations of 4–4, 4–5, and 5–4, whereas Very High hydroclimatic stress corresponds to the 5–5 combination. All remaining combinations are classified as Other. Classes were defined relative to the historical baseline (1991–2010) (Figure related to Table A4).

## 4. Discussion

### *4.1. Evolution of Precipitation and Hydroclimatic Extremes*

Projected changes in precipitation and precipitation-related climate indices consistently indicate a progressive intensification of hydroclimatic extremes across the Iberian Peninsula, with the magnitude of change strongly dependent on the emission pathway. The projected decline in annual precipitation, particularly under SSP3–7.0 and SSP5–8.5, agrees with previous studies identifying the Mediterranean Basin as a climate-change hotspot undergoing progressive aridification because of the poleward displacement of Atlantic storm tracks and the expansion of subtropical high-pressure systems [3,39–42]. The strongest drying is projected for southern and interior Iberia, whereas Atlantic-influenced northwestern regions remain comparatively wetter, reflecting the well-established climatic gradient across the Peninsula [15]. These contrasting responses suggest increasing pressure on regional water availability, reservoir recharge and ecosystem functioning, particularly under limited climate mitigation.

The projected evolution reflects the combined influence of time horizon and scenario forcing rather than a uniform response to either factor alone. Differences among SSPs are comparatively limited during 2041–2060 but become progressively more pronounced toward 2081–2100, when SSP3–7.0 and particularly SSP5–8.5 produce greater and more spatially extensive changes. This divergence is also geographically heterogeneous, with southern and southwestern Iberia showing the earliest and strongest intensification and a progressive extension of elevated hydroclimatic stress toward interior and central basins, while northern and northwestern regions generally exhibit weaker responses.

The projected increase in CDD complements these precipitation changes by indicating a widespread tendency towards longer uninterrupted dry periods, especially across southern and interior Iberia. Rather than representing drought directly, CDD provides an indicator of increasingly prolonged dry spells that may constrain soil moisture replenishment and surface water availability. Similar tendencies have been reported for Mediterranean Europe under future warming scenarios [24,41]. The pronounced increase in CDD under SSP3–7.0 and SSP5–8.5 therefore suggests increasing pressure on agricultural production, reservoir recharge, groundwater resources and ecosystem resilience [41–43]. Moreover, the clear divergence between mitigation pathways highlights the strong influence of greenhouse-gas emissions on the future maximum duration of uninterrupted dry conditions across the Peninsula [39].

Additional insight is provided by the joint interpretation of CDD and CDDn. Although CDDn decreases across parts of southern Iberia, this should not be interpreted as an improvement in hydroclimatic conditions. Instead, when analysed together with the simultaneous increase in CDD, these changes indicate a transition from numerous shorter dry spells towards fewer but longer dry episodes. In contrast, the projected increase in CDDn across eastern and northeastern Iberia suggests greater fragmentation of dry conditions, characterised by more frequent dry spells [32,40,41]. These contrasting regional responses demonstrate that climate change is expected to modify not only the duration but also the temporal organisation of dry conditions across the Peninsula. Consequently, future hydroclimatic regimes are likely to become increasingly heterogeneous, with southern regions dominated by longer uninterrupted dry periods, while eastern sectors experience more fragmented but recurrent dry conditions. The marked differences among emission scenarios further demonstrate the potential benefits of climate mitigation in limiting these changes.

The projected evolution of the fraction of R95pTOT indicates that annual precipitation is expected to become increasingly concentrated into a limited number of very wet days, particularly under SSP3–7.0 and SSP5–8.5. It is important to note that an increase in the fraction of R95pTOT does not necessarily imply an increase in the absolute amount of extreme precipitation, but rather that a larger proportion of the annual precipitation total occurs during relatively few intense rainfall events. Such a redistribution reflects increasingly irregular precipitation regimes, even where annual precipitation declines [43]. This behaviour is consistent with the thermodynamic response of a warmer atmosphere, which enhances its moisture-holding capacity and favours more intense precipitation episodes when rainfall occurs [44]. Consequently, future precipitation regimes across the IP are expected to become progressively more concentrated, potentially increasing runoff generation, flash-flood occurrence, soil erosion and sediment transport while reducing infiltration efficiency and effective groundwater recharge [16].

### *4.2. Hydroclimatic Stress Framework and Implications for River-Basin Management*

Beyond the individual evolution of precipitation and hydroclimatic indices, the combined hydroclimatic stress framework provides an integrated perspective of future climate pressures across the IP. By jointly evaluating the highest historical quintiles of CDD and the fraction of R95pTOT, the framework identifies regions jointly exposed to prolonged dry periods and increasing temporal concentration of precipitation. Although these conditions do not represent temporally concurrent compound events, their spatial coexistence within the same river basins indicates increasing hydroclimatic pressure that may complicate long-term water-resource management.

The widespread occurrence of the upper fractional R95pTOT classes in some southern basins should be interpreted as an increasing concentration of the annual precipitation budget on historically very wet days, rather than as evidence of increasing absolute extreme-

precipitation amounts. Moreover, because the classification is based on fixed historical quintile thresholds, once a large proportion of a basin exceeds an upper-class boundary, the categorical representation becomes less sensitive to further changes in the underlying continuous variable. Conversely, shifts between adjacent High and Very High classes may result from relatively modest changes around the historical class boundary and should therefore not be interpreted as abrupt changes in hydroclimatic conditions. The distinction between High and Very High combined hydroclimatic stress introduced in this study partly addresses this threshold sensitivity by retaining information from both upper quintile classes rather than relying exclusively on the simultaneous occurrence of the two Very High classes. In the Guadalquivir and Guadiana basins, where the fraction of R95pTOT is already saturated in the "Very High" class from the earliest scenario and time slice, variation in the combined-stress classification is therefore effectively driven by changes in the CDD classification.

The basin-scale analysis demonstrates that hydroclimatic stress is not uniformly distributed across the Peninsula but progressively concentrates within southern and interior watersheds. The Guadalquivir and Guadiana basins consistently emerge as the most vulnerable systems, followed by the Tagus basin, whereas the Atlantic-influenced Douro basin and much of the Ebro basin remain comparatively less exposed, despite exhibiting increasing hydroclimatic stress under the higher-emission scenarios. This north–south contrast reflects the combined influence of decreasing precipitation, increasing recurrence and magnitude of dry conditions, and greater concentration of annual rainfall into relatively few intense events, reinforcing the well-documented climatic transition from Atlantic to Mediterranean environments [3,15,39–42].

From a water-management perspective, these projected changes suggest that future adaptation strategies should account not only for reductions in water availability but also for increasing variability in the temporal distribution of precipitation. Longer dry periods may reduce reservoir inflows, groundwater recharge and soil-moisture recovery, whereas the increasing concentration of annual precipitation into a limited number of intense rainfall events may enhance runoff generation and reduce the efficiency with which precipitation contributes to water storage [45,46]. Reservoir operation rules, irrigation systems, urban drainage infrastructure, and flood-protection measures may become increasingly inadequate under future hydroclimatic variability [25,39,42–44]. Consequently, southern Iberian basins may experience increasing difficulty in balancing water supply, agricultural demand, flood protection and ecosystem requirements under future climate conditions.

The watershed-scale approach adopted in this study further demonstrates the value of hydrologically meaningful management units for climate-impact assessments. Because river basins constitute the operational units for water planning under the European WFD, evaluating hydroclimatic stress at this scale provides information directly relevant for reservoir operation, drought planning and long-term adaptation strategies [25,45–47]. The progressive expansion of hydroclimatic stress under SSP3–7.0 and especially SSP5–8.5 further highlights the potential benefits of climate mitigation, as lower-emission pathways substantially limit the spatial extent of the most vulnerable areas.

Although it provides a consistent assessment of projected hydroclimatic changes across the IP, this study has limitations. An important limitation is that CDD and CDDn are precipitation-based indicators and therefore do not account for warming-driven increases in atmospheric evaporative demand. Consequently, they should not be interpreted as comprehensive measures of agricultural or hydrological drought. Under future warming, comparable dry-spell characteristics may be associated with greater soil-moisture depletion and crop water stress owing to increased evapotranspiration. Incorporating temperature-sensitive indicators such as SPEI, evapotranspiration, soil moisture, streamflow, or related hydrological variables would therefore provide a more complete assessment of future

water stress. The hydroclimatic stress framework is based on the spatial concurrence of the highest historical quintiles of CDD and the fraction of R95pTOT and, therefore, identifies regions simultaneously exposed to an increasing number of dry spells and precipitation concentration rather than temporally concurrent compound events [48–50]. The framework is also region-dependent, as the historical quintile thresholds are derived for the entire study domain and may therefore not fully represent local hydroclimatic conditions. Consequently, the framework should be interpreted as an indicator of cumulative hydroclimatic pressure at the basin scale rather than a representation of the chronological interaction between dry and wet extremes. Furthermore, although the use of a multi-model CMIP6 ensemble combined with the CHELSA–ISIMIP3b high-resolution dataset reduces the influence of individual model biases, uncertainties associated with climate-model structure, emission scenarios, and downscaling methodologies remain inherent to future climate projections and should be considered when interpreting the results. However, the use of a multi-model ensemble and multiple scenarios increases the robustness of the results. Despite these limitations, the present study provides a robust and spatially explicit assessment of future hydroclimatic stress conditions across the IP. Southern and interior Iberian basins emerge as particularly vulnerable hotspots where future climate change may severely challenge water security, ecosystem resilience, and long-term socio-economic sustainability [51,52].

Future research could extend the proposed framework by incorporating additional hydroclimatic indicators representing other dimensions of climate variability, such as precipitation intensity, soil-moisture dynamics or hydrological drought, together with impact-based variables including streamflow, reservoir storage or groundwater recharge. Coupling the hydroclimatic stress framework with hydrological and water-allocation models would also enable the translation of projected climate changes into quantitative estimates of water availability and sector-specific vulnerability. Such developments would provide a more comprehensive basis for evaluating adaptation strategies and supporting integrated water-resource management under future climate change, both across the IP and in other Mediterranean regions facing similar hydroclimatic challenges.

## 5. Conclusions

This study provides a high-resolution assessment of projected hydroclimatic change across the IP by integrating changes in mean annual precipitation, CDD, CDDn, and the fraction of R95pTOT. The projections indicate a progressive intensification of hydroclimatic pressures through the century, particularly under SSP3–7.0 and SSP5–8.5. Mean annual precipitation declines most strongly across southern and interior Iberia, locally exceeding 30% under SSP5–8.5 by 2081–2100, while CDD increases substantially and exceeds 90 days $yr^{-1}$ in parts of southern Iberia. CDDn exhibits a different spatial response, increasing mainly across eastern and northeastern regions while remaining stable or decreasing locally in the south, indicating that future drying may increasingly be expressed through fewer but longer uninterrupted dry periods. At the same time, the increasing fraction of R95pTOT indicates a greater concentration of the annual precipitation budget on historically very wet days.

The river-basin analysis reveals a pronounced spatial contrast in the magnitude of these changes. Under SSP5–8.5 during 2081–2100, the “Very High” CDD class is projected to encompass 97.08% of the Guadalquivir basin, 94.80% of the Guadiana and 71.12% of the Tagus, compared with 24.23% of the Douro and 0% of the Ebro. The combined hydroclimatic stress framework further strengthens this differentiation. By 2081–2100 under SSP5–8.5, 97.08% of the Guadalquivir and 94.80% of the Guadiana are classified as “Very High” combined hydroclimatic stress. In the Tagus, 64.56% of the basin reaches “Very High” stress and a further 29.53% is classified as “High”, meaning that approximately 94% of its area is projected to experience at least “High” combined stress. The Douro exhibits a more

moderate but nevertheless substantial response, with 24.23% of its area reaching the "Very High" CDD class and, in the combined assessment, 45.57% classified as "High" and 0.58% as "Very High" stress by 2061–2080 under SSP5–8.5, indicating an emerging expansion of elevated hydroclimatic stress into this Atlantic-influenced basin. In contrast, the Ebro remains outside the "Very High" combined-stress category by 2081–2100, although 18.74% of its area reaches "High" stress. These results identify the Guadalquivir and Guadiana as the most consistently exposed major basins, while the Tagus shows a particularly marked transition toward increasingly widespread upper stress classes and the Douro displays an emerging, although less severe, intensification of combined hydroclimatic stress.

Overall, the results show that future hydroclimatic change across the IP is characterised not only by increasing dryness, but by the spatial coexistence of increasingly prolonged dry periods and a greater concentration of annual precipitation on historically very wet days. This combination is particularly pronounced in southern and interior river basins and creates potentially competing challenges for water storage, supply reliability and management of intense precipitation. The strong contrast between the lower- and higher-emission projections toward the end of the century further indicates that the magnitude and spatial extent of these pressures remain sensitive to future radiative forcing. The basin-scale patterns identified here therefore provide a quantitative basis for prioritising climate adaptation and water-resource planning, particularly in the Guadalquivir, Guadiana and Tagus basins, while highlighting the importance of accounting for both prolonged dry conditions and increasingly concentrated precipitation in future river-basin management.

**Author Contributions:** Conceptualization, C.A., A.F. (André Fonseca) and J.A.S.; methodology, C.A.; validation, C.A., A.F. (André Fonseca), A.F. (António Fernandes), C.M. and J.A.S.; formal analysis, C.A.; investigation, C.A.; resources, C.A.; data curation, C.A., A.F. (André Fonseca), A.F. (António Fernandes) and C.M.; writing—original draft preparation, C.A.; writing—review and editing, C.A., A.F. (André Fonseca), A.F. (António Fernandes), C.M. and J.A.S.; visualization, C.A.; funding acquisition, C.A. All authors have read and agreed to the published version of the manuscript.

**Funding:** This work is supported by National Funds by FCT—Portuguese Foundation for Science and Technology, under the projects UID/04033/2025: Centre for the Research and Technology of Agro-Environmental and Biological Sciences (https://doi.org/10.54499/UID/04033/2025) and LA/P/0126/2020 (https://doi.org/10.54499/LA/P/0126/2020).

**Data Availability Statement:** The CHELSA V2.1 climate datasets used in this study are publicly available through the CHELSA (Climatologies at High Resolution for the Earth's Land Surface Areas) database at https://www.chelsa-climate.org/ (accessed on 15 June 2025). Further inquiries can be directed to the corresponding author.

**Acknowledgments:** During the preparation of this manuscript, the author(s) used chatGPT-5.6 Sol (OpenAI) for the purposes of improving grammar, spelling, and language clarity. The graphical abstract is the only figure for which generative AI was used. The authors have reviewed and edited the output and take full responsibility for the content of this publication.

**Conflicts of Interest:** The authors declare no conflicts of interest.

## Abbreviations

The following abbreviations are used in this manuscript:

| | |
|---|---|
| CDD | Consecutive Dry Days |
| CDDn | Number of Dry Spells |
| CHELSA | Climatologies at High Resolution for the Earth's Land Surface Areas |
| CMIP6 | Coupled Model Intercomparison Project Phase 6 |

| | |
|---|---|
| EU | European Union |
| GCM | Global Climate Model |
| HydroBASINS | Hydrological Watershed Boundaries Dataset |
| IP | Iberian Peninsula |
| ISIMIP3b | Inter-Sectoral Impact Model Intercomparison Project Phase 3b |
| NUTS | Nomenclature of Territorial Units for Statistics |
| PR | Precipitation |
| R95pTOT | Very Wet Days |
| SPEI | Standardised Precipitation Evapotranspiration Index |
| SPI | Standardised Precipitation Index |
| SSP | Shared Socioeconomic Pathway |
| SSP1–2.6 | Sustainability Pathway (Low emissions) |
| SSP3–7.0 | Regional Rivalry Pathway (Medium-high emissions) |
| SSP5–8.5 | Fossil-Fuelled Development Pathway (High emissions) |
| WFD | EU Water Framework Directive |

# Appendix A

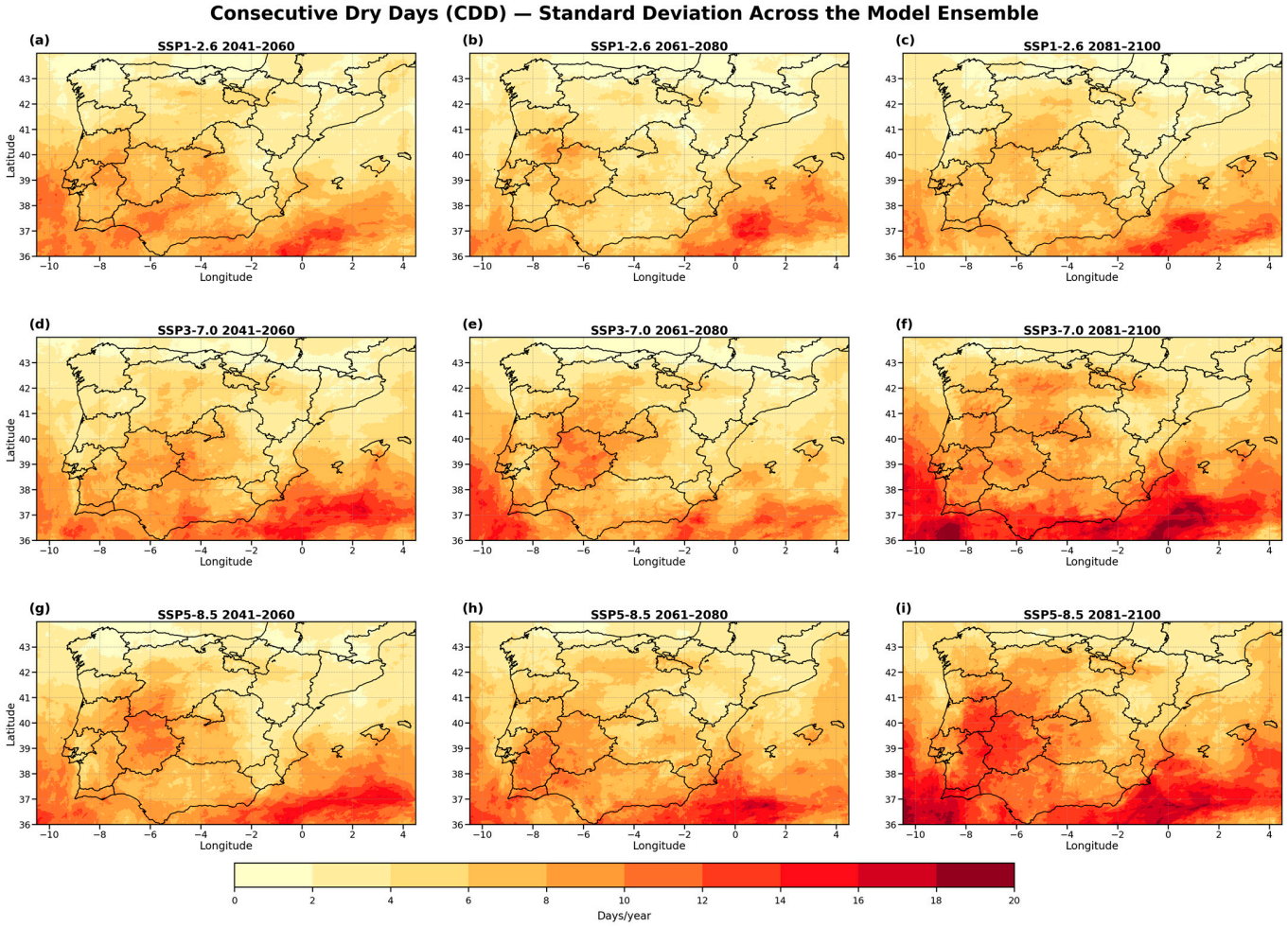



**Figure A1.** Spatial distribution of the inter-model standard deviation of Consecutive Dry Days (CDD) across the nine-member CHELSA–ISIMIP3b CMIP6 ensemble over the Iberian Peninsula. Rows correspond to the Shared Socioeconomic Pathways SSP1–2.6 (**a**–**c**), SSP3–7.0 (**d**–**f**), and SSP5–8.5 (**g**–**i**), while columns represent the future periods 2041–2060 (**a**,**d**,**g**), 2061–2080 (**b**,**e**,**h**), and 2081–2100 (**c**,**f**,**i**). Standard deviation is expressed in days/year, with higher values indicating greater inter-model spread in projected CDD. A common colour scale is used across all panels to facilitate comparison among scenarios and time horizons.

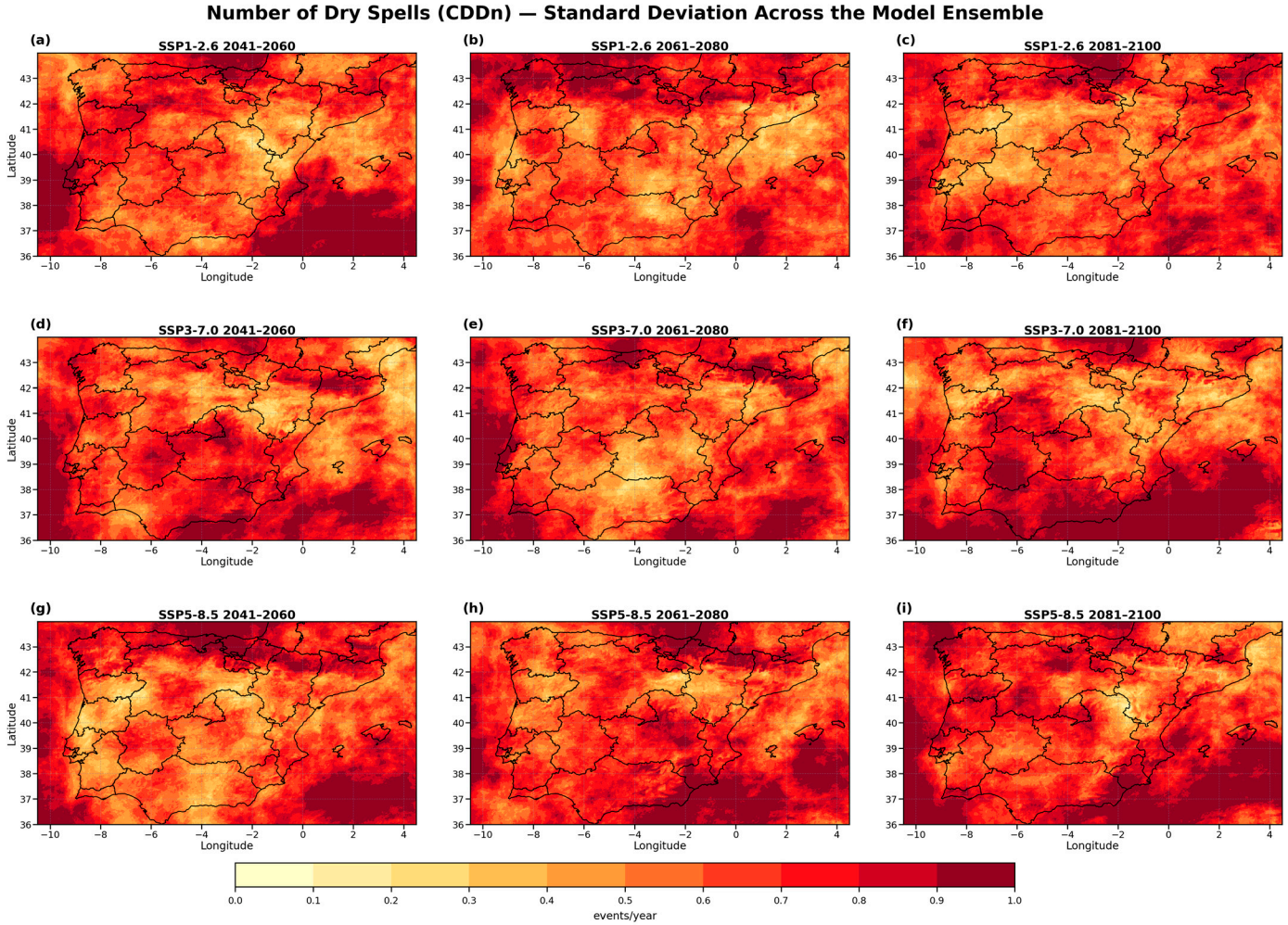



**Figure A2.** Spatial distribution of the inter-model standard deviation of the Number of Dry Spells (CDDn) across the nine-member CHELSA–ISIMIP3b CMIP6 ensemble over the Iberian Peninsula. Rows correspond to the Shared Socioeconomic Pathways SSP1–2.6 (**a**–**c**), SSP3–7.0 (**d**–**f**), and SSP5–8.5 (**g**–**i**), while columns represent the future periods 2041–2060 (**a**,**d**,**g**), 2061–2080 (**b**,**e**,**h**), and 2081–2100 (**c**,**f**,**i**). Standard deviation is expressed in events/year, with higher values indicating greater inter-model spread in projected dry-spell recurrence. A common colour scale is used across all panels to facilitate comparison among scenarios and time horizons.

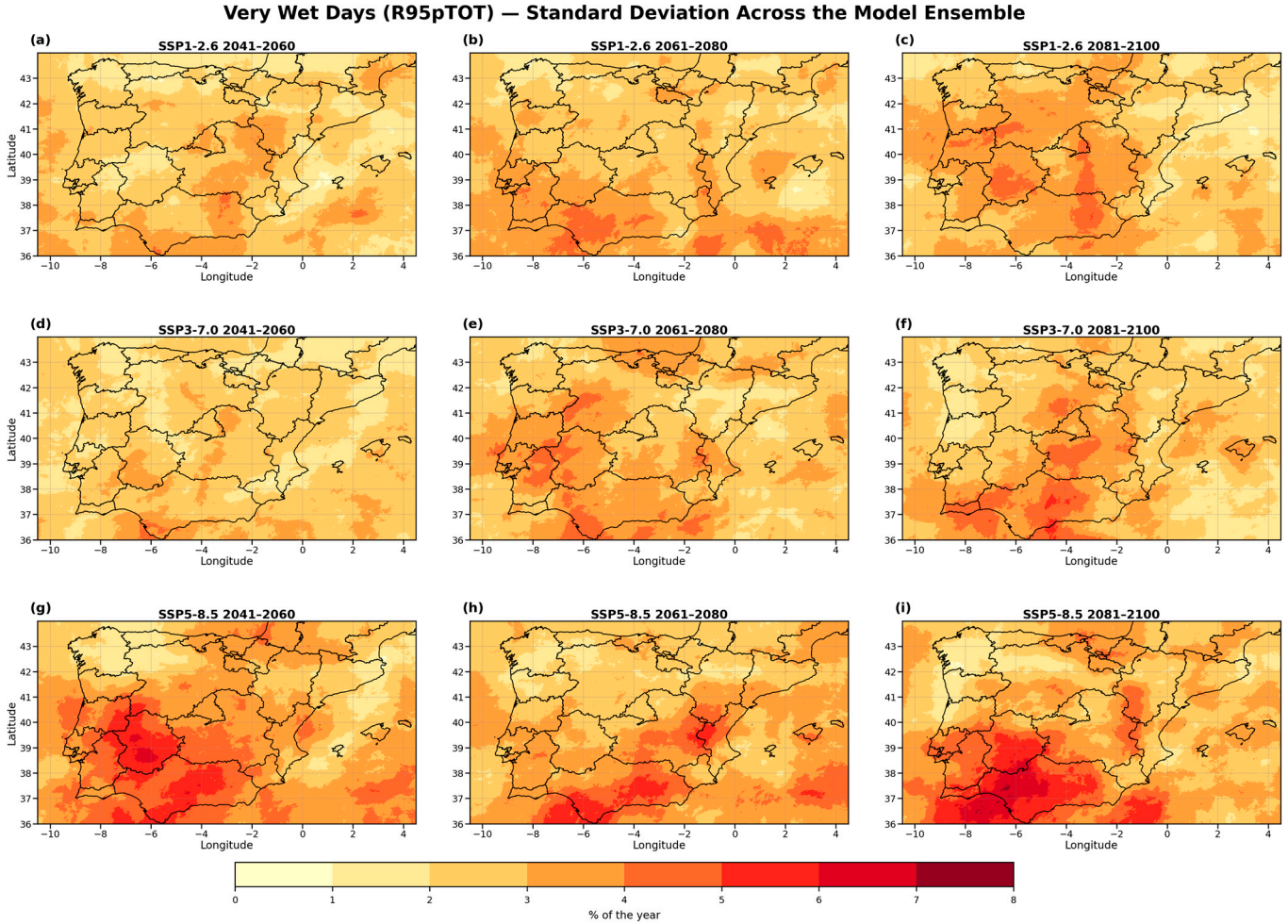



**Figure A3.** Spatial distribution of the inter-model standard deviation of the fraction of precipitation from Very Wet Days (R95pTOT) across the nine-member CHELSA–ISIMIP3b CMIP6 ensemble over the Iberian Peninsula. Rows correspond to the Shared Socioeconomic Pathways SSP1–2.6 (**a**–**c**), SSP3–7.0 (**d**–**f**), and SSP5–8.5 (**g**–**i**), while columns represent the future periods 2041–2060 (**a**,**d**,**g**), 2061–2080 (**b**,**e**,**h**), and 2081–2100 (**c**,**f**,**i**). Standard deviation is expressed in percentage points of annual precipitation, with higher values indicating greater inter-model spread in the projected contribution of historically very wet days to annual precipitation. A common colour scale is used across all panels to facilitate comparison among scenarios and time horizons.

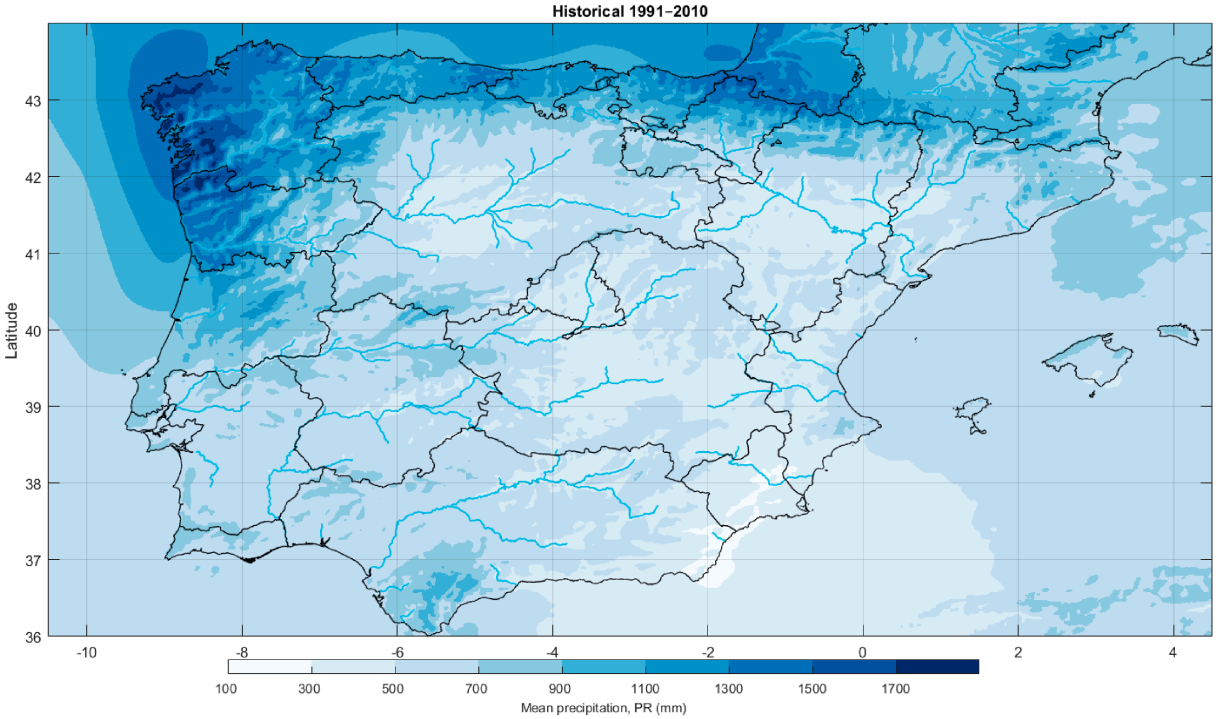



**Figure A4.** Spatial distribution of mean annual precipitation (PR; mm $yr^{-1}$) across the Iberian Peninsula for the historical baseline period 1991–2010. Values represent the nine-model CHELSA–ISIMIP3b CMIP6 ensemble mean.

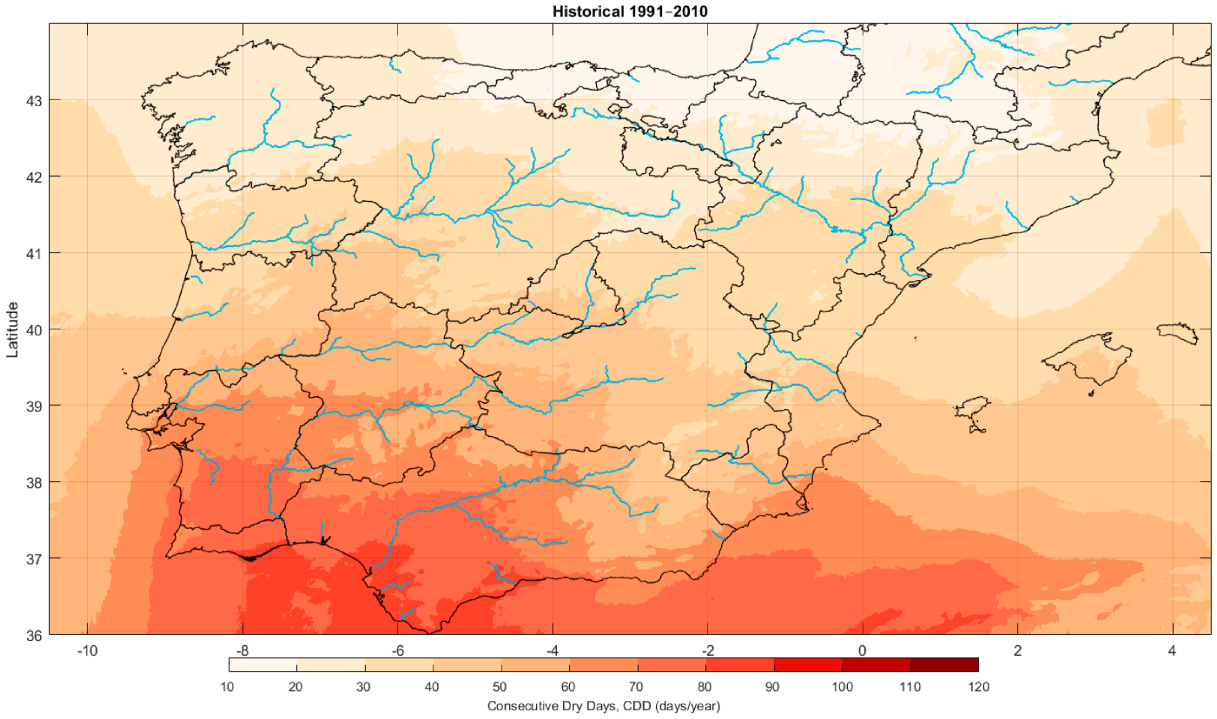



**Figure A5.** Spatial distribution of mean annual Consecutive Dry Days (CDD; days $yr^{-1}$) across the Iberian Peninsula for the historical baseline period 1991–2010. CDD represents the annual maximum number of consecutive days with daily precipitation below 1 mm. Values represent the nine-model CHELSA–ISIMIP3b CMIP6 ensemble mean.

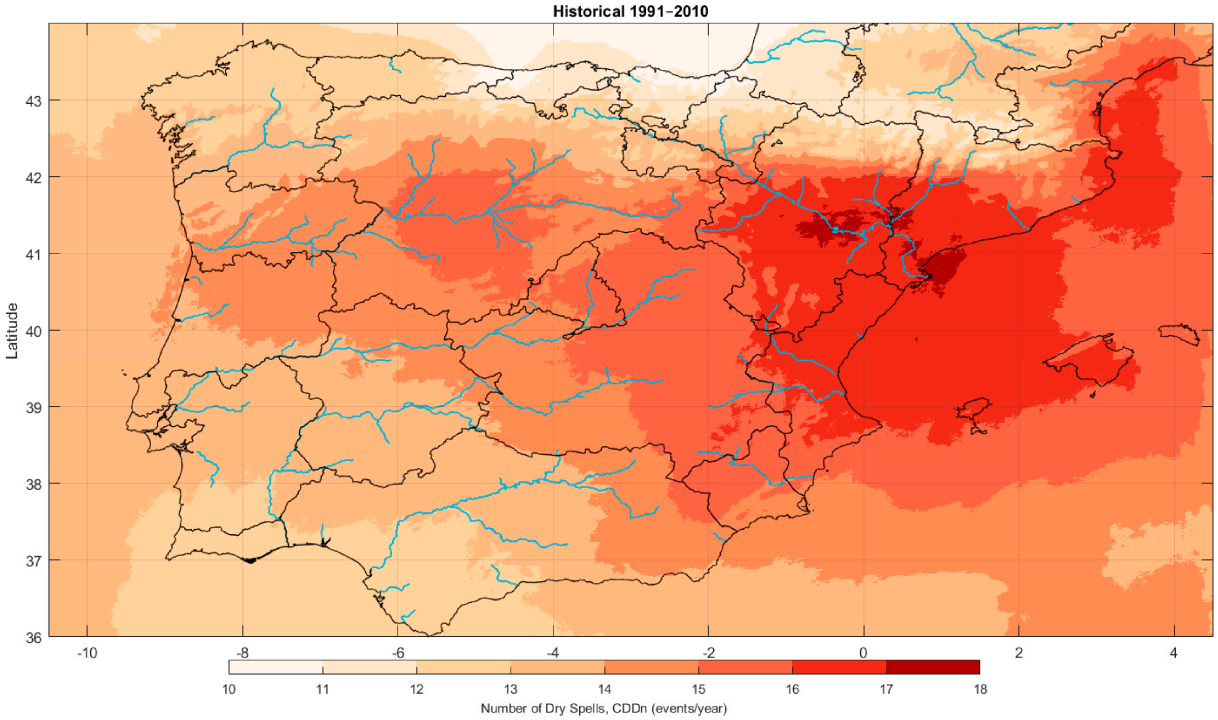



**Figure A6.** Spatial distribution of the mean annual Number of Dry Spells (CDDn; events $yr^{-1}$) across the Iberian Peninsula for the historical baseline period 1991–2010. CDDn represents the annual number of dry spells exceeding five consecutive days with daily precipitation below 1 mm. Values represent the nine-model CHELSA–ISIMIP3b CMIP6 ensemble mean.

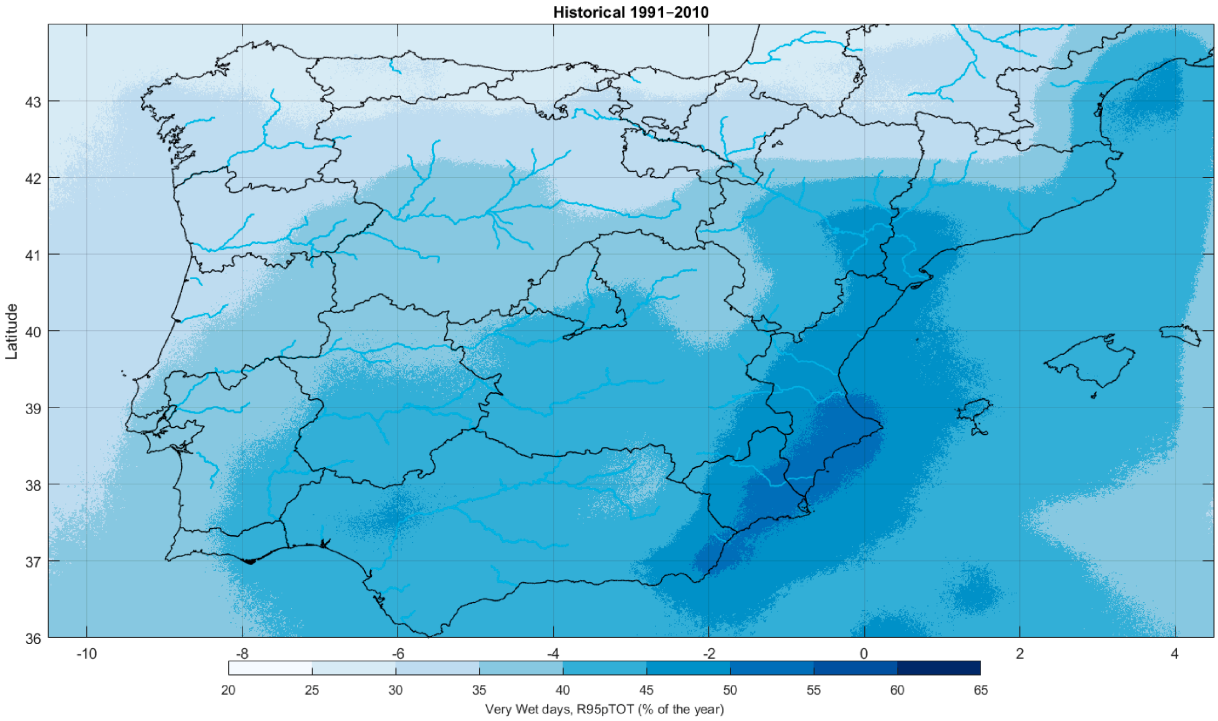



**Figure A7.** Spatial distribution of the mean fraction of R95pTOT (%) across the Iberian Peninsula for the historical baseline period 1991–2010. The index represents the percentage of annual precipitation occurring on days exceeding the grid-cell-specific 95th-percentile daily precipitation threshold derived from the 1981–2010 reference period. Values represent the nine-model CHELSA–ISIMIP3b CMIP6 ensemble mean.

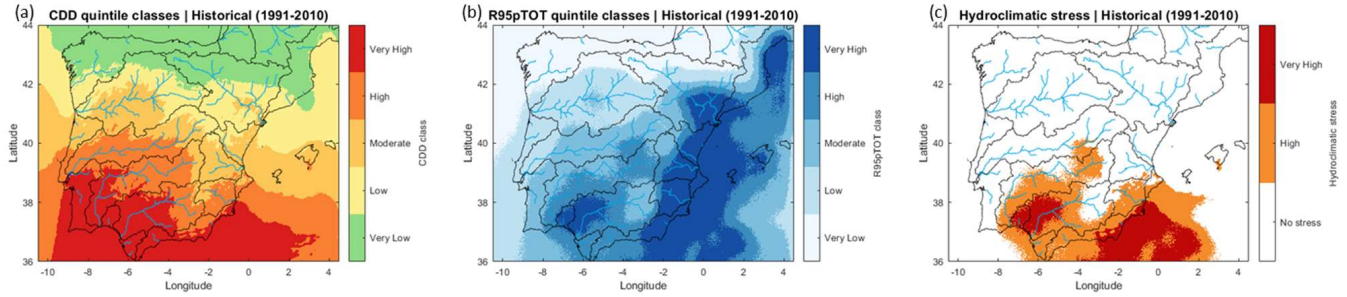



**Figure A8.** Historical spatial distribution of (**a**) CDD quintile classes, (**b**) fraction of R95pTOT quintile classes, and (**c**) combined hydroclimatic stress across the Iberian Peninsula for the 1991–2010 baseline period. Quintile thresholds for CDD and the fraction of R95pTOT were derived independently from the spatial distribution of their 1991–2010 climatological mean values across all Iberian grid cells. Combined hydroclimatic stress is classified as High for the CDD–R95pTOT combinations 4–4, 4–5, and 5–4, and Very High for the 5–5 combination; all remaining combinations are classified as Other.

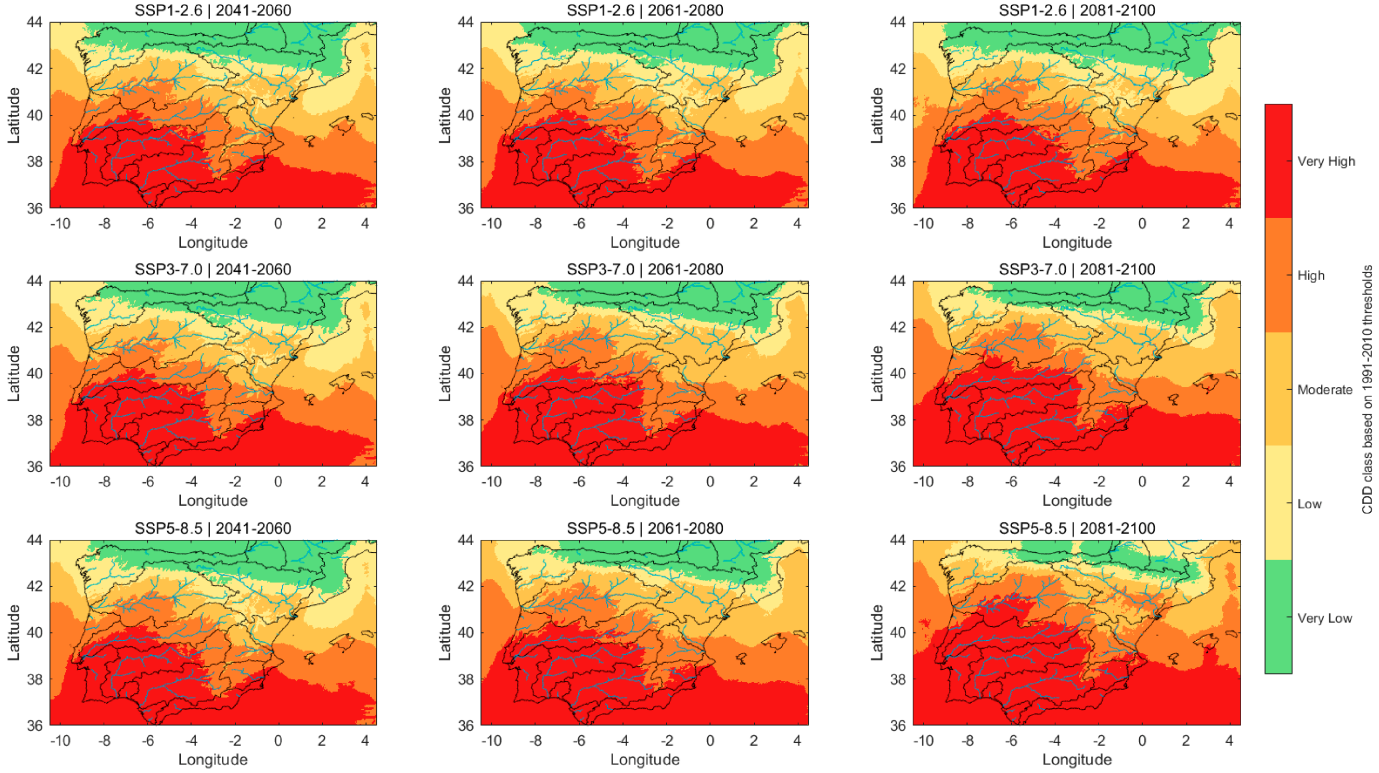



**Figure A9.** Projected spatial distribution of CDD quintile classes across the Iberian Peninsula under SSP1–2.6 (**top** row), SSP3–7.0 (**middle** row), and SSP5–8.5 (**bottom** row) for 2041–2060, 2061–2080, and 2081–2100. Future values were classified using fixed CDD quintile thresholds derived from the spatial distribution of the 1991–2010 historical climatological mean values.

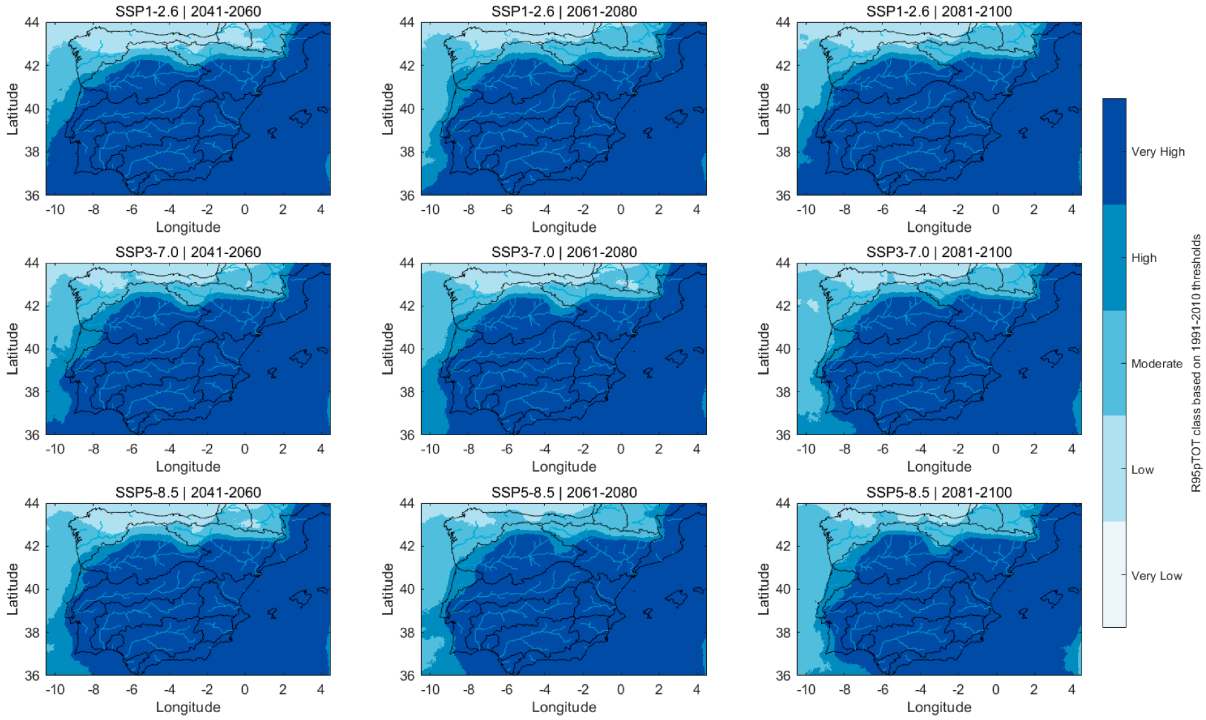



**Figure A10.** Projected spatial distribution of the fraction of R95pTOT quintile classes across the Iberian Peninsula under SSP1–2.6 (**top** row), SSP3–7.0 (**middle** row), and SSP5–8.5 (**bottom** row) for 2041–2060, 2061–2080, and 2081–2100. Future values were classified using fixed fraction-of-R95pTOT quintile thresholds derived from the spatial distribution of the 1991–2010 historical climatological mean values.

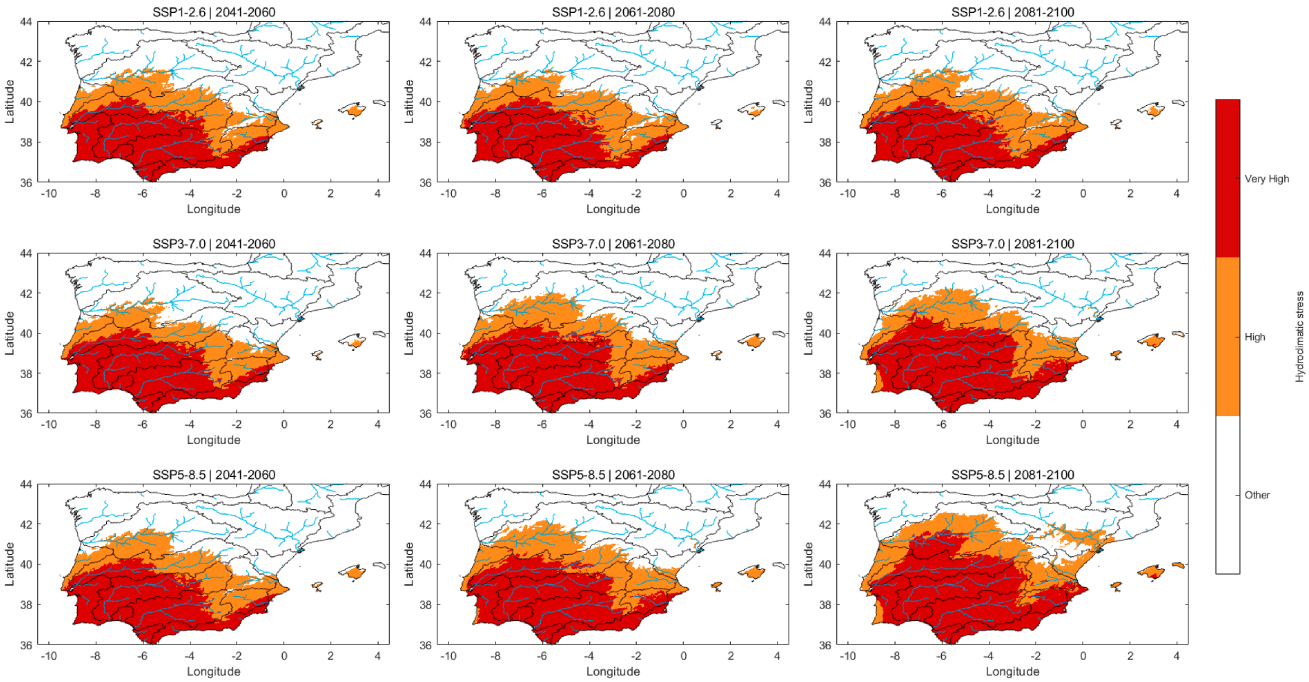



**Figure A11.** Projected spatial distribution of combined hydroclimatic stress across the Iberian Peninsula under SSP1–2.6 (**top** row), SSP3–7.0 (**middle** row), and SSP5–8.5 (**bottom** row) for 2041–2060, 2061–2080, and 2081–2100. High hydroclimatic stress corresponds to CDD–fraction of R95pTOT class combinations 4–4, 4–5, and 5–4, whereas Very High stress corresponds to the 5–5 combination. All remaining combinations are classified as Other. Classes are defined relative to the fixed 1991–2010 historical spatial quintile thresholds.

**Table A1.** Main geographical and hydrological characteristics of the major river basins considered in this study, including basin area, transboundary status, and selected water-resource attributes relevant to the assessment of hydroclimatic stress across the Iberian Peninsula [53–55].

| River 2. | Basin Area (km$^2$) | Main River Length (km) | Countries | Description |
|---|---|---|---|---|
| Douro | 98,073 | 897 | Spain, Portugal | Largest Iberian basin; major transboundary water-management unit |
| Ebro | 85,534 | 930 | Andorra, Spain, Portugal | Largest predominantly Spanish basin and main Mediterranean-draining basin |
| Tagus | 80,500 | 1100 | Spain, Portugal | Longest Iberian River and major transboundary basin |
| Guadiana | 67,773 | 744 | Spain, Portugal | Large transboundary basin with substantial exposure to water scarcity |
| Guadalquivir | 57,527 | 657 | Spain | Major southern Iberian basin with high agricultural water demand |

**Table A2.** Percentage of grid cells (%) within each CDD hydroclimatic stress class (Very Low to Very High) for the main Iberian watersheds under SSP1–2.6, SSP3–7.0, and SSP5–8.5 during the future periods 2041–2060, 2061–2080, and 2081–2100 (Table related to Figure 12).

| Scenario | Period | Watershed | Very Low | Low | Moderate | High | Very High |
|---|---|---|---|---|---|---|---|
| SSP1–2.6 | 2041–2060 | Ebro | 37.70 | 33.79 | 28.51 | 0.00 | 0.00 |
| | | Guadalquivir | 0.00 | 0.00 | 0.69 | 15.72 | 83.59 |
| | | Guadiana | 0.00 | 0.00 | 1.02 | 24.44 | 74.54 |
| | | Tagus | 0.00 | 2.16 | 20.46 | 52.80 | 24.58 |
| | | Douro | 5.66 | 21.82 | 46.77 | 25.76 | 0.00 |
| SSP1–2.6 | 2061–2080 | Ebro | 41.70 | 39.48 | 18.82 | 0.00 | 0.00 |
| | | Guadalquivir | 0.00 | 0.00 | 0.48 | 22.01 | 77.51 |
| | | Guadiana | 0.00 | 0.00 | 0.82 | 30.53 | 68.65 |
| | | Tagus | 0.00 | 6.23 | 19.54 | 46.15 | 28.08 |
| | | Douro | 7.88 | 26.12 | 45.33 | 20.67 | 0.00 |
| SSP1–2.6 | 2081–2100 | Ebro | 41.31 | 39.41 | 19.28 | 0.00 | 0.00 |
| | | Guadalquivir | 0.00 | 0.00 | 0.35 | 19.18 | 80.47 |
| | | Guadiana | 0.00 | 0.00 | 1.37 | 28.91 | 69.72 |
| | | Tagus | 0.00 | 4.71 | 20.71 | 50.19 | 24.40 |
| | | Douro | 7.45 | 24.46 | 45.18 | 22.91 | 0.00 |
| SSP3–7.0 | 2041–2060 | Ebro | 39.87 | 31.79 | 28.34 | 0.00 | 0.00 |
| | | Guadalquivir | 0.00 | 0.00 | 0.06 | 15.93 | 84.01 |
| | | Guadiana | 0.00 | 0.00 | 0.84 | 23.36 | 75.80 |
| | | Tagus | 0.00 | 4.50 | 21.88 | 46.28 | 27.33 |
| | | Douro | 6.29 | 24.88 | 46.94 | 21.89 | 0.00 |
| SSP3–7.0 | 2061–2080 | Ebro | 31.69 | 24.61 | 43.69 | 0.00 | 0.00 |
| | | Guadalquivir | 0.00 | 0.00 | 0.00 | 13.22 | 86.78 |
| | | Guadiana | 0.00 | 0.00 | 0.04 | 15.53 | 84.44 |
| | | Tagus | 0.00 | 0.01 | 15.89 | 40.26 | 43.85 |
| | | Douro | 3.56 | 12.94 | 42.44 | 40.90 | 0.15 |

**Table A2.** *Cont.*

| Scenario | Period | Watershed | Very Low | Low | Moderate | High | Very High |
|---|---|---|---|---|---|---|---|
| SSP3–7.0 | 2081–2100 | Ebro | 26.06 | 24.49 | 48.68 | 0.77 | 0.00 |
| | | Guadalquivir | 0.00 | 0.00 | 0.00 | 7.44 | 92.56 |
| | | Guadiana | 0.00 | 0.00 | 0.00 | 11.12 | 88.88 |
| | | Tagus | 0.00 | 0.00 | 11.39 | 26.69 | 61.92 |
| | | Douro | 2.83 | 8.14 | 36.90 | 47.85 | 4.28 |
| SSP5–8.5 | 2041–2060 | Ebro | 38.37 | 37.27 | 24.35 | 0.00 | 0.00 |
| | | Guadalquivir | 0.00 | 0.00 | 0.34 | 17.89 | 81.78 |
| | | Guadiana | 0.00 | 0.00 | 0.63 | 25.54 | 73.83 |
| | | Tagus | 0.00 | 3.21 | 19.30 | 45.23 | 32.25 |
| | | Douro | 6.51 | 23.99 | 39.22 | 30.28 | 0.00 |
| SSP5–8.5 | 2061–2080 | Ebro | 25.63 | 26.20 | 47.75 | 0.43 | 0.00 |
| | | Guadalquivir | 0.00 | 0.00 | 0.00 | 9.60 | 90.40 |
| | | Guadiana | 0.00 | 0.00 | 0.04 | 16.79 | 83.17 |
| | | Tagus | 0.00 | 0.00 | 14.92 | 38.47 | 46.61 |
| | | Douro | 2.81 | 8.09 | 42.91 | 45.61 | 0.58 |
| SSP5–8.5 | 2081–2100 | Ebro | 12.09 | 21.79 | 47.34 | 18.78 | 0.00 |
| | | Guadalquivir | 0.00 | 0.00 | 0.00 | 2.92 | 97.08 |
| | | Guadiana | 0.00 | 0.00 | 0.00 | 5.20 | 94.80 |
| | | Tagus | 0.00 | 0.00 | 5.91 | 22.97 | 71.12 |
| | | Douro | 0.67 | 4.23 | 19.16 | 51.70 | 24.23 |

**Table A3.** Percentage of grid cells (%) within each R95pTOT hydroclimatic stress class (Very Low to Very High) for the main Iberian watersheds under SSP1–2.6, SSP3–7.0, and SSP5–8.5 during the future periods 2041–2060, 2061–2080, and 2081–2100 (Table related to Figure 13).

| Scenario | Period | Watershed | Very Low | Low | Moderate | High | Very High |
|---|---|---|---|---|---|---|---|
| SSP1–2.6 | 2041–2060 | Ebro | 0.00 | 6.29 | 26.61 | 9.20 | 57.90 |
| | | Guadalquivir | 0.00 | 0.00 | 0.00 | 0.00 | 100.00 |
| | | Guadiana | 0.00 | 0.00 | 0.00 | 0.00 | 100.00 |
| | | Tagus | 0.00 | 0.00 | 0.00 | 0.00 | 100.00 |
| | | Douro | 0.00 | 4.94 | 12.39 | 20.10 | 62.57 |
| SSP1–2.6 | 2061–2080 | Ebro | 0.00 | 0.26 | 30.84 | 10.45 | 58.45 |
| | | Guadalquivir | 0.00 | 0.00 | 0.00 | 0.00 | 100.00 |
| | | Guadiana | 0.00 | 0.00 | 0.00 | 0.00 | 100.00 |
| | | Tagus | 0.00 | 0.00 | 0.00 | 0.05 | 99.95 |
| | | Douro | 0.00 | 0.67 | 12.25 | 22.18 | 64.91 |
| SSP1–2.6 | 2081–2100 | Ebro | 0.00 | 0.38 | 27.59 | 11.88 | 60.19 |
| | | Guadalquivir | 0.00 | 0.00 | 0.00 | 0.00 | 100.00 |
| | | Guadiana | 0.00 | 0.00 | 0.00 | 0.00 | 100.00 |
| | | Tagus | 0.00 | 0.00 | 0.00 | 0.00 | 100.00 |
| | | Douro | 0.00 | 2.56 | 9.82 | 18.09 | 69.53 |
| SSP3–7.0 | 2041–2060 | Ebro | 0.00 | 0.81 | 29.61 | 10.83 | 58.75 |
| | | Guadalquivir | 0.00 | 0.00 | 0.00 | 0.00 | 100.00 |
| | | Guadiana | 0.00 | 0.00 | 0.00 | 0.00 | 100.00 |
| | | Tagus | 0.00 | 0.00 | 0.00 | 2.69 | 97.31 |
| | | Douro | 0.00 | 0.17 | 12.26 | 22.62 | 64.95 |
| SSP3–7.0 | 2061–2080 | Ebro | 0.00 | 1.16 | 30.92 | 9.39 | 58.53 |
| | | Guadalquivir | 0.00 | 0.00 | 0.00 | 0.00 | 100.00 |
| | | Guadiana | 0.00 | 0.00 | 0.00 | 0.00 | 100.00 |
| | | Tagus | 0.00 | 0.00 | 0.00 | 0.25 | 99.75 |
| | | Douro | 0.00 | 2.81 | 11.41 | 21.67 | 64.11 |

**Table A3.** *Cont.*

| Scenario | Period | Watershed | Very Low | Low | Moderate | High | Very High |
|---|---|---|---|---|---|---|---|
| SSP3–7.0 | 2081–2100 | Ebro | 0.00 | 0.15 | 22.99 | 14.43 | 62.44 |
| | | Guadalquivir | 0.00 | 0.00 | 0.00 | 0.00 | 100.00 |
| | | Guadiana | 0.00 | 0.00 | 0.00 | 0.00 | 100.00 |
| | | Tagus | 0.00 | 0.00 | 4.05 | 95.95 | 0.00 |
| | | Douro | 0.00 | 0.72 | 11.63 | 19.75 | 67.89 |
| SSP5–8.5 | 2041–2060 | Ebro | 0.00 | 2.61 | 28.59 | 9.88 | 58.92 |
| | | Guadalquivir | 0.00 | 0.00 | 0.00 | 0.00 | 100.00 |
| | | Guadiana | 0.00 | 0.00 | 0.00 | 0.00 | 100.00 |
| | | Tagus | 0.00 | 0.00 | 0.00 | 0.01 | 99.99 |
| | | Douro | 0.00 | 2.39 | 10.87 | 20.88 | 65.86 |
| SSP5–8.5 | 2061–2080 | Ebro | 0.00 | 0.00 | 22.70 | 15.95 | 61.35 |
| | | Guadalquivir | 0.00 | 0.00 | 0.00 | 0.00 | 100.00 |
| | | Guadiana | 0.00 | 0.00 | 0.00 | 0.00 | 100.00 |
| | | Tagus | 0.00 | 0.00 | 0.00 | 1.64 | 98.36 |
| | | Douro | 0.00 | 0.00 | 7.04 | 22.55 | 70.41 |
| SSP5–8.5 | 2081–2100 | Ebro | 0.00 | 0.26 | 26.93 | 11.52 | 61.30 |
| | | Guadalquivir | 0.00 | 0.00 | 0.00 | 0.00 | 100.00 |
| | | Guadiana | 0.00 | 0.00 | 0.00 | 0.00 | 100.00 |
| | | Tagus | 0.00 | 0.00 | 0.00 | 6.56 | 93.44 |
| | | Douro | 0.00 | 0.07 | 9.97 | 22.11 | 67.86 |

**Table A4.** Percentage of grid cells (%) within the "Very High" hydroclimatic stress class for the main Iberian watersheds under SSP1–2.6, SSP3–7.0, and SSP5–8.5 during the future periods 2041–2060, 2061–2080, and 2081–2100 (Table related to Figure 14).

| Scenario | Period | Watershed | Very Low | High | Very High |
|---|---|---|---|---|---|
| SSP1–2.6 | 2041–2060 | Ebro | 100.00 | 0.00 | 0.00 |
| | | Guadalquivir | 0.69 | 15.72 | 83.59 |
| | | Guadiana | 1.02 | 24.45 | 74.53 |
| | | Tagus | 22.64 | 52.81 | 24.56 |
| | | Douro | 74.30 | 25.70 | 0.00 |
| SSP1–2.6 | 2061–2080 | Ebro | 100.00 | 0.00 | 0.00 |
| | | Guadalquivir | 0.48 | 22.03 | 77.50 |
| | | Guadiana | 0.82 | 30.55 | 68.63 |
| | | Tagus | 25.78 | 46.14 | 28.07 |
| | | Douro | 79.36 | 20.64 | 0.00 |
| SSP1–2.6 | 2081–2100 | Ebro | 100.00 | 0.00 | 0.00 |
| | | Guadalquivir | 0.35 | 19.19 | 80.46 |
| | | Guadiana | 1.37 | 28.92 | 69.71 |
| | | Tagus | 25.43 | 50.19 | 24.39 |
| | | Douro | 77.11 | 22.89 | 0.00 |
| SSP3–7.0 | 2041–2060 | Ebro | 100.00 | 0.00 | 0.00 |
| | | Guadalquivir | 0.06 | 15.93 | 84.01 |
| | | Guadiana | 0.85 | 23.36 | 75.79 |
| | | Tagus | 26.40 | 46.34 | 27.26 |
| | | Douro | 78.14 | 21.86 | 0.00 |

**Table A4.** *Cont.*

| Scenario | Period | Watershed | Very Low | High | Very High |
|---|---|---|---|---|---|
| SSP3–7.0 | 2061–2080 | Ebro | 100.00 | 0.00 | 0.00 |
| | | Guadalquivir | 0.00 | 13.23 | 86.77 |
| | | Guadiana | 0.04 | 15.53 | 84.43 |
| | | Tagus | 15.91 | 40.26 | 43.82 |
| | | Douro | 58.96 | 40.89 | 0.15 |
| SSP3–7.0 | 2081–2100 | Ebro | 99.23 | 0.77 | 0.00 |
| | | Guadalquivir | 0.00 | 7.45 | 92.55 |
| | | Guadiana | 0.00 | 11.12 | 88.88 |
| | | Tagus | 11.40 | 30.16 | 58.45 |
| | | Douro | 48.28 | 47.45 | 4.27 |
| SSP5–8.5 | 2041–2060 | Ebro | 100.00 | 0.00 | 0.00 |
| | | Guadalquivir | 0.34 | 17.90 | 81.76 |
| | | Guadiana | 0.64 | 25.54 | 73.82 |
| | | Tagus | 22.53 | 45.24 | 32.23 |
| | | Douro | 69.74 | 30.26 | 0.00 |
| SSP5–8.5 | 2061–2080 | Ebro | 99.58 | 0.42 | 0.00 |
| | | Guadalquivir | 0.00 | 9.61 | 90.39 |
| | | Guadiana | 0.04 | 16.80 | 83.16 |
| | | Tagus | 14.93 | 39.49 | 45.58 |
| | | Douro | 53.86 | 45.57 | 0.58 |
| SSP5–8.5 | 2081–2100 | Ebro | 81.26 | 18.74 | 0.00 |
| | | Guadalquivir | 0.00 | 2.92 | 97.08 |
| | | Guadiana | 0.00 | 5.20 | 94.80 |
| | | Tagus | 5.91 | 29.53 | 64.56 |
| | | Douro | 25.97 | 51.00 | 23.03 |

## References


1. Vicente-Serrano, S.M.; Beguería, S.; López-Moreno, J.I. A multiscalar drought index sensitive to global warming: The Standardized Precipitation Evapotranspiration Index. *J. Clim.* **2010**, *23*, 1696–1718. [CrossRef]
2. García-Ruiz, J.M.; López-Moreno, J.I.; Vicente-Serrano, S.M.; Lasanta–Martínez, T.; Beguería, S. Mediterranean water resources in a global change scenario. *Earth-Sci. Rev.* **2011**, *105*, 121–139. [CrossRef]
3. Guerreiro, S.B.; Dawson, R.J.; Kilsby, C.; Lewis, E.; Ford, A. Future heat–waves, droughts and floods in 571 European cities. *Environ. Res. Lett.* **2018**, *13*, 034009. [CrossRef]
4. Lelieveld, J.; Hadjinicolaou, P.; Kostopoulou, E.; Chenoweth, J.; El Maayar, M.; Giannakopoulos, C.; Hannides, C.; Lange, M.A.; Tanarhte, M.; Tyrlis, E.; et al. Climate change and impacts in the Eastern Mediterranean and the Middle East. *Clim. Change* **2012**, *114*, 667–687. [CrossRef] [PubMed]
5. Sousa, P.M.; Trigo, R.M.; Barriopedro, D.; Soares, P.M.M.; Santos, J.A. European temperature responses to blocking and ridge regional patterns. *Clim. Dyn.* **2018**, *50*, 457–477. [CrossRef]
6. Benetó, P.; Valiente, J.A.; Khodayar, S. Exploring shifts in extreme precipitation and synoptic forces across the Iberian Peninsula: A regionalized perspective. *Weather Clim. Extrem.* **2026**, *53*, 100929. [CrossRef]
7. Pereira, S.C.; Carvalho, D.; Rocha, A. Temperature and Precipitation Extremes over the Iberian Peninsula under Climate Change Scenarios: A Review. *Climate* **2021**, *9*, 139. [CrossRef]
8. Fonseca, A.; Andrade, C.; Santos, J.A. Agricultural Water Security under Climate Change in the Iberian Peninsula. *Water* **2022**, *14*, 768. [CrossRef]
9. Fonseca, A.; Cruz, J.; Andrade, C.; Fernandes, A.; Menz, C.; Santos, J.A. High-resolution climate-driven potential evapotranspiration to assess climate change impacts on Mediterranean agriculture. *Front. Clim.* **2026**, *8*, 1854734. [CrossRef]
10. Iglesias, A.; Garrote, L.; Flores, F.; Moneo, M. Challenges to manage the risk of water scarcity and climate change in the Mediterranean. *Water Resour. Manag.* **2007**, *21*, 775–788. [CrossRef]
11. Claro, A.M.; Fonseca, A.; Fraga, H.; Santos, J.A. Susceptibility of Iberia to Extreme Precipitation and Aridity: A New High-Resolution Analysis over an Extended Historical Period. *Water* **2023**, *15*, 3840. [CrossRef]

12. Estrela, T.; Pérez-Martín, M.A.; Vargas, E. Impacts of climate change on water resources in Spain. *Hydrol. Sci. J.* **2012**, *57*, 1154–1167. [CrossRef]
13. Andrade, C.; Contente, J. Köppen–Geiger Climate Classification Projections for the Iberian Peninsula. *Clim. Res.* **2020**, *81*, 71–89. [CrossRef]
14. Gampe, D.; Nikulin, G.; Ludwig, R. Using an ensemble of regional climate models to assess climate change impacts on water scarcity in European river basins. *Sci. Total Environ.* **2016**, *573*, 1503–1518. [CrossRef] [PubMed]
15. Herrera, S.; Gutiérrez, J.M.; Ancell, R.; Pons, M.R.; Frías, M.D.; Fernández, J. Development and analysis of a 50-year high-resolution daily gridded precipitation dataset over Spain (Spain02). *Int. J. Climatol.* **2012**, *32*, 74–85. [CrossRef]
16. Zscheischler, J.; Westra, S.; van den Hurk, B.; Seneviratne, S.I.; Ward, P.J.; Pitman, A.; AghaKouchak, A.; Bresch, D.N.; Leonard, M.; Wahl, T.; et al. Future climate risk from compound events. *Nat. Clim. Chang.* **2018**, *8*, 469–477. [CrossRef]
17. Bevacqua, E.; De Michele, C.; Manning, C.; Couasnon, A.; Ribeiro, A.F.S.; Ramos, A.M.; Vignotto, E.; Bastos, A.; Blesić, S.; Durante, F.; et al. Guidelines for studying diverse types of compound weather and climate events. *Earth's Future* **2021**, *9*, e2021EF002340. [CrossRef]
18. Ridder, N.; de Vries, H.; Drijfhout, S. The role of atmospheric rivers in compound events consisting of heavy precipitation and high storm surges along the Dutch coast. *Nat. Hazards Earth Syst. Sci.* **2018**, *18*, 3311–3326. [CrossRef]
19. Ridder, N.N.; Pitman, A.J.; Westra, S.; Ukkola, A.; Do, H.X.; Bador, M.; Hirsch, A.L.; Evans, J.P.; Di Luca, A.; Zscheischler, J. Global hotspots for the occurrence of compound events. *Nat. Commun.* **2020**, *11*, 5956. [CrossRef] [PubMed]
20. Stagge, J.H.; Kingston, D.G.; Tallaksen, L.M.; Hannah, D.M. Observed drought indices show increasing divergence across Europe. *Sci. Rep.* **2017**, *7*, 14045. [CrossRef] [PubMed]
21. Zhang, X.; Alexander, L.; Hegerl, G.C.; Jones, P.; Tank, A.K.; Peterson, T.C.; Trewin, B.; Zwiers, F.W. Indices for monitoring changes in extremes based on daily temperature and precipitation data. *WIREs Clim. Change* **2011**, *2*, 851–870. [CrossRef]
22. Beguería, S.; Vicente-Serrano, S.M.; Angulo-Martínez, M. A Multiscalar Global Drought Dataset: The SPEIbase: A New Gridded Product for the Analysis of Drought Variability and Impacts. *Bull. Am. Meteorol. Soc.* **2010**, *91*, 1351–1356. [CrossRef]
23. Riahi, K.; van Vuuren, D.P.; Kriegler, E.; Edmonds, J.; O'Neill, B.C.; Fujimori, S.; Bauer, N.; Calvin, K.; Dellink, R.; Fricko, O.; et al. The Shared Socioeconomic Pathways and their energy, land use, and greenhouse gas emissions implications: An overview. *Glob. Environ. Change* **2017**, *42*, 153–168. [CrossRef]
24. Tramblay, Y.; Koutroulis, A.; Samaniego, L.; Vicente-Serrano, S.M.; Volaire, F.; Boone, A.; Le Page, M.; Llasat, C.M.; Albergel, C.; Burak, S.; et al. Challenges for drought assessment in the Mediterranean region under future climate scenarios. *Earth-Sci. Rev.* **2020**, *210*, 103348. [CrossRef]
25. European Parliament and Council. Directive 2000/60/EC of the European Parliament and of the Council Establishing a Framework for Community Action in the Field of Water Policy. *Off. J. Eur. Communities* **2000**, *L327*, 1–73. Available online: https://eur-lex.europa.eu/legal-content/EN/TXT/?uri=CELEX%3A32000L0060 (accessed on 15 June 2025).
26. Lehner, B.; Grill, G. Global river hydrography and network routing: Baseline data and new approaches to study the world's large river systems. *Hydrol. Processes* **2013**, *27*, 2171–2186. [CrossRef]
27. Eyring, V.; Bony, S.; Meehl, G.A.; Senior, C.A.; Stevens, B.; Stouffer, R.J.; Taylor, K.E. Overview of the Coupled Model Intercomparison Project Phase 6 (CMIP6) experimental design and organization. *Geosci. Model Dev.* **2016**, *9*, 1937–1958. [CrossRef]
28. Frieler, K.; Volkholz, J.; Lange, S.; Schewe, J.; Mengel, M.; Del Rocío Rivas López, M.; Otto, C.; Reyer, C.P.O.; Karger, D.N.; Malle, J.T.; et al. Scenario Setup and Forcing Data for Impact Model Evaluation and Impact Attribution within the Third Round of the Inter-Sectoral Impact Model Intercomparison Project (ISIMIP3a). *Geosci. Model Dev.* **2024**, *17*, 1–51. [CrossRef]
29. Lange, S. ISIMIP3b Bias Adjustment Fact Sheet. 2021. Available online: https://www.isimip.org/ (accessed on 15 June 2025).
30. Lange, S. *ISIMIP3BASD*, version 2.5.0; Zenodo: Geneva, Switzerland, 2021. [CrossRef]
31. Lange, S. Trend-Preserving Bias Adjustment and Statistical Downscaling with ISIMIP3BASD (v1.0). *Geosci. Model Dev.* **2019**, *12*, 3055–3070. [CrossRef]
32. Lindenlaub, L.; Weigel, K.; Hassler, B.; Jones, C.; Eyring, V. Characteristics of Agricultural Droughts in CMIP6 Historical Simulations and Future Projections. *Earth Syst. Dyn.* **2026**, *17*, 81–105. [CrossRef]
33. O'Neill, B.C.; Tebaldi, C.; Van Vuuren, D.P.; Eyring, V.; Friedlingstein, P.; Hurtt, G.; Knutti, R.; Kriegler, E.; Lamarque, J.F.; Lowe, J.; et al. The Scenario Model Intercomparison Project (ScenarioMIP) for CMIP6. *Geosci. Model Dev.* **2016**, *9*, 3461–3482. [CrossRef]
34. Karger, D.N.; Conrad, O.; Böhner, J.; Kawohl, T.; Kreft, H.; Soria-Auza, R.W.; Zimmermann, N.E.; Linder, H.P.; Kessler, M. Climatologies at high resolution for the earth's land surface areas. *Sci. Data* **2017**, *4*, 170122. [CrossRef] [PubMed]
35. Karger, D.N.; Wilson, A.M.; Mahony, C.; Zimmermann, N.E.; Jetz, W. Global daily 1 km land surface precipitation based on cloud cover-informed downscaling. *Sci. Data* **2021**, *8*, 307. [CrossRef] [PubMed]
36. Sillmann, J.; Kharin, V.V.; Zwiers, F.W.; Zhang, X.; Bronaugh, D. Climate extremes indices in the CMIP5 multimodel ensemble: Part 2. Future climate projections. *J. Geophys. Res. Atmos.* **2013**, *118*, 2473–2493. [CrossRef]
37. Nicholls, N.; Alexander, L. Has the climate become more variable or extreme? Progress 1992–2006. *Prog. Phys. Geogr.* **2007**, *31*, 1–11. [CrossRef]

38. Spinoni, J.; Naumann, G.; Vogt, J. Pan-European seasonal trends and recent changes of drought frequency and severity. *Glob. Planet. Change* **2017**, *148*, 113–130. [CrossRef]
39. Seneviratne, S.I.; Nicholls, N.; Easterling, D.; Goodess, C.M.; Kanae, S.; Kossin, J.; Luo, Y.; Marengo, J.; McInnes, K.; Rahimi, M.; et al. Changes in climate extremes and their impacts on the natural physical environment. In *Managing the Risks of Extreme Events and Disasters to Advance Climate Change Adaptation*; Field, C.B., Barros, V., Stocker, T.F., Qin, D., Dokken, D.J., Ebi, K.L., Mastrandrea, M.D., Mach, K.J., Plattner, G.-K., Allen, S.K., et al., Eds.; A Special Report of Working Groups I and II of the Intergovernmental Panel on Climate Change (IPCC); Cambridge University Press: Cambridge, UK; New York, NY, USA, 2012; pp. 109–230. Available online: https://www.ipcc.ch/report/srex/ (accessed on 15 June 2025).
40. Doshi, S.C.; Lohmann, G.; Ionita, M. Hotspot movement of compound events on the Europe continent. *Sci. Rep.* **2023**, *13*, 18100. [CrossRef] [PubMed]
41. Vogel, J.; Paton, E.; Aich, V.; Bronstert, A. Increasing Compound Warm Spells and Droughts in the Mediterranean Basin. *Weather Clim. Extrem.* **2021**, *32*, 100312. [CrossRef]
42. Jacob, D.; Kotova, L.; Teichmann, C.; Sobolowski, S.P.; Vautard, R.; Donnelly, C.; Koutroulis, A.; Grillakis, M.; Tsanis, I.K.; Damm, A.; et al. Climate Impacts in Europe Under +1.5 °C Global Warming. *Earth's Future* **2018**, *6*, 264–285. [CrossRef]
43. Betts, R.A.; Alfieri, L.; Bradshaw, C.; Caesar, J.; Feyen, L.; Friedlingstein, P.; Gohar, L.; Koutroulis, A.; Lewis, K.; Morfopoulos, C.; et al. Changes in climate extremes, fresh water availability and vulnerability to food insecurity projected at 1.5 °C and 2 °C global warming with a higher-resolution global climate model. *Philos. Trans. R. Soc. A Math. Phys. Eng. Sci.* **2018**, *376*, 20160452. [CrossRef] [PubMed]
44. Seneviratne, S.I.; Zhang, X.; Adnan, M.; Badi, W.; Dereczynski, C.; Di Luca, A.; Ghosh, S.; Iskandar, I.; Kossin, J.; Lewis, S.; et al. Weather and Climate Extreme Events in a Changing Climate. In *Climate Change 2021: The Physical Science Basis: Working Group I to the Sixth Assessment Report of the Intergovernmental Panel on Climate Change*; Masson-Delmotte, V., Zhai, P., Pirani, A., Connors, S.L., Péan, C., Berger, S., Caud, N., Chen, Y., Goldfarb, L., Gomis, M.I., et al., Eds.; Cambridge University Press: Cambridge, UK; New York, NY, USA, 2021; pp. 1513–1766. [CrossRef]
45. Andrade, C.; Contente, J. Climate Change Projections for the Worldwide Bioclimatic Classification System in the Iberian Peninsula until 2070. *Int. J. Climatol.* **2020**, *40*, 5863–5886. [CrossRef]
46. Paredes-Beltran, B.; Sordo-Ward, A.; Martin-Carrasco, F.; Garrote, L. High-resolution estimates of water availability for the Iberian Peninsula under climate scenarios. *Appl. Water Sci.* **2024**, *14*, 167. [CrossRef]
47. Estrela, T.; Vargas, E. Effects of climate change on hydrological resources in Europe: The case of Spain. In *Global Warming and Climate Change, Prospects and Policies in Asia and Europe*; Marquina, A., Ed.; Palgrave Macmillan: Basingstoke, UK; New York, NY, USA, 2010.
48. Vargas-Amelin, E.; Pindado, P. The Challenge of Climate Change in Spain: Water Resources, Agriculture and Land. *J. Hydrol.* **2014**, *518*, 243–249. [CrossRef]
49. González-Cao, J.; Fernández-Nóvoa, D.; deCastro, N.G.; Barreiro-Fonta, H.; deCastro, M.; Gómez-Gesteira, M. Impact of dams on river regime and extreme flow events in MIÑO–SIL river basin (NW of the IBERIAN peninsula). *CATENA* **2026**, *264*, 109836. [CrossRef]
50. Ceballos-Barbancho, A. Water resources and environmental change in a Mediterranean environment: The south-west sector of the Duero River basin (Spain). *J. Hydrol.* **2008**, *351*, 126–138. [CrossRef]
51. Pascual, D.; Pla, E.; Lopez-Bustins, J.A.; Retana, J.; Terradas, J. Impacts of climate change on water resources in the Mediterranean Basin: A case study in Catalonia, Spain. *Hydrol. Sci. J.* **2015**, *60*, 2132–2147. [CrossRef]
52. Murray, S.J.; Foster, P.N.; Prentice, I.C. Future global water resources with respect to climate change and water withdrawals as estimated by a dynamic global vegetation model. *J. Hydrol.* **2012**, *448–449*, 14–29. [CrossRef]
53. Santisteban, J.I.; Schulte, L. Fluvial networks of the Iberian Peninsula: A chronological framework. *Quat. Sci. Rev.* **2007**, *26*, 2738–2757. [CrossRef]
54. Ramos, A.M.; Trigo, R.M.; Liberato, M.; Tomé, R. Daily Precipitation Extreme Events in the Iberian Peninsula and Its Association with Atmospheric Rivers. *J. Hydrometeorol.* **2015**, *16*, 579–597. [CrossRef]
55. Bravo-Paredes, N.; Gallego, M.C.; Vaquero, J.M.; Trigo, R.M. The catastrophic floods in the Guadiana River basin since 1500 CE. *Sci. Total Environ.* **2021**, *797*, 149141. [CrossRef] [PubMed]


**Disclaimer/Publisher's Note:** The statements, opinions and data contained in all publications are solely those of the individual author(s) and contributor(s) and not of MDPI and/or the editor(s). MDPI and/or the editor(s) disclaim responsibility for any injury to people or property resulting from any ideas, methods, instructions or products referred to in the content.